International Journal of Steel Structures (2023) 23(1):96–119
https://doi.org/10.1007/s13296-022-00681-4

Online ISSN 2093-6311
Print ISSN 1598-2351

Effectiveness of Fan Anchors in Preventing Debonding in FRP-Strengthened Steel Members

Esmaeel Esmaeeli[1] · **Parisa Shadan**[2]

Received: 15 January 2022 / Accepted: 23 September 2022 / Published online: 21 October 2022

Abstract
Fibre Reinforced Polymers (FRPs) are extensively employed to strengthen existing structures because of their several advantages over other strengthening techniques. On the other hand, the premature debonding of FRP reduces its effectiveness in strengthening steel structures. Anchoring FRP composites is an effective solution to delay or even prevent their debonding. Very limited anchorage methods, however, have been introduced for FRP-strengthened steel structures and the need for an effective anchorage system remains. Fan anchor has been validated as one of the remedies against debonding failure in FRP-strengthened concrete structures. Considering the advantages that fan anchors offer, the use of fan anchors for FRP-strengthened steel structures is proposed and evaluated in this paper. Since FRP-steel joints have a different bond-slip law than FRP-concrete joints and the strengthened steel members are prone to buckling-debonding interactions, this study focuses on the efficiency of fan anchors in delaying FRP debonding by assuming that an adequate mechanical connection between the dowel and the steel substrate is provided. Three experimental studies involving shear, flexural and buckling strengthening of steel components were simulated through finite element modelling, and fan anchors were added to the models after validation. The effect of fan anchors on strength, failure mode and FRP's strain distribution of the models was examined. The study showed that the fan anchor was successfully able to delay debonding mode, which increased the strength and ductility and exploited a higher strain capacity of FRP plates.

Keywords Debonding · Fan anchor · FRP-strengthening · Steel structures · FE modelling

1 Introduction

Over time, the rehabilitation of steel structures such as bridges, pipelines and buildings has become vital. However, conventional rehabilitation methods such as plate replacing and welding/bolting steel plates, which are widely used for local repair, suffer from inflexibility, weight increase, corrosion and residual stresses caused by welding (Teng et al., 2012). Fibre Reinforced Polymers (FRP), which have a high strength-to-weight ratio, good corrosion resistance, fatigue resistance, and shape flexibility, have received much attention in recent years as a viable alternative to steel patch for the rehabilitation of steel structures (Zhao & Zhang, 2007).

While FRP's ability to strengthen concrete structures has been proven over the years (Naser et al., 2019; F. Shadan et al., 2015), its efficiency in enhancing the performance of steel structures is still under investigation (P. Shadan & Kabir, 2018c; Q.-Q. Yu & Wu, 2018; Zhao & Zhang, 2007; Zheng et al., 2021). One problem that questions the applicability of FRP composites for steel structures is the weak bond between FRP and steel surfaces caused by high-stress concentration (Smith & Teng, 2001). As reported by previous studies, in the majority of cases, premature debonding of FRP from steel surface hindered FRP effectiveness, and the strengthening capacity of composite remained considerably underutilised (Buyukozturk et al., 2004; Dilum Fernando, 2010; P. Shadan & Kabir, 2018b; Sivaganesh & Mahendrakumar, 2019). The study by Fernando et al. (2010) on FRP-strengthening of fatigue-damaged steel girders demonstrated the role of debonding in the rate of crack propagation in steel beams. The premature debonding of the FRP patch was also claimed to be the first failure mode in FRP patch repaired cracked steel plates (Tsouvalis et al., 2009). Shaat and

✉ Esmaeel Esmaeeli
esmaeel.esmaeeli@brunel.ac.uk

[1] Department of Civil and Environmental Engineering, Brunel University London, London, UK

[2] Centre for Infrastructure Engineering, Western Sydney University, Sydney, Australia

Fam (2006) stated the premature debonding of FRP from a buckled face as the most observed failure mode in the FRP-strengthened SHS columns tested under axial loading. This failure mode was also observed in all FRP-strengthened steel tubular members tested under the lateral impact (Alam et al., 2017). Through the strengthening of SHS braces, Shadan and Kabir (2018a) remarked on the impotent behaviour of the strengthened braces after the debonding of FRP from an inward buckled face.

Only a few studies have been dedicated to resolving the issue of premature debonding in FRP-strengthened steel structures. Some researchers employed anchoring bolts (Sweedan et al., 2013, 2016) as well as their combination with steel plates or angles (Li et al., 2018; Yang et al., 2021) to inhibit premature debonding of FRP from steel plates. In addition, a few types of metallic anchors, such as G-shaped Clamps, were introduced for the anchorage of plate-end debonding (Katrizadeh & Narmashiri, 2019; Sen et al., 2001; Y. Wang & Zhou, 2017). Some other techniques such as internal taper, adhesive fillet and enhancing epoxy adhesion have also been suggested to postpone the occurrence of premature debonding (F M da Silva & D Adams, 2007; B. Wang et al., 2016). Additionally, thick-walled sections were utilised at the ends of FRP plates to overcome the plate-end debonding in FRP-strengthened steel tubes (Liu et al., 2021). Nevertheless, most of the suggested techniques were specifically designed for plate-end debonding and are not applicable to other modes of deboning. Furthermore, as the proposed anchors are made of steel, the inherent inflexibility of steel limits their application, and they are liable to corrosion. In addition, high stress concentration at sharp edges of steel anchors could result in premature rupture of FRP composites (D. et al., 2002). Therefore, the need for an efficient anchorage system with a flexible shape and ability to utilise FRP composite's highest capacity remains.

In accordance with previous research, fan anchors have been found as a highly efficient solution for anchoring FRP-concrete joints (Q. Wang et al., 2020).

Fan anchors, also called FRP dowels, fibre bolts and FRP spike anchors, are made from bundled fibres and consist of two parts of fan and dowel (See Fig. 1). The fan part is splayed in a fan or circular shape and epoxied to the FRP surface, responsible for transferring the FRP's tensile force to the dowel. The dowel is bonded into a predrilled hole in the concrete substrate to transfer the load to concrete (Zhang et al., 2012). When a debonding failure at the FRP-concrete interface initiates, the fan anchor is activated, providing a new stress transfer mechanism whereby FRP debonding is postponed.

Fan anchors can be constructed using two methods: dry and impregnated. In dry anchors no epoxy is applied to rolled fibres during the manufacturing process, while in the latter, the dowel part of rolled fibres is impregnated with epoxy in the manufacturing stage (Zhang et al., 2012). Fan anchors are small, easy to install and flexible in shape, hence applicable to a wide variety of structural components (Kalfat et al., 2013). Moreover, compared with metallic anchors, the FRP nature of fan anchors allows for a better bond with the FRP substrate. It was also proved that the use of fan anchors increases the strain efficiency of FRP plates, and the level of strain improvement depends on the scale and quantity of fan anchors (Zhang & Smith, 2012).

In this paper, a novel employment of fan anchors in FRP-strengthened steel members is proposed and investigated through a numerical study. Three different experimental studies in which FRP was employed for shear strengthening, flexural strengthening, and buckling strengthening of steel elements were chosen to evaluate the efficiency of fan anchors at different loading conditions. First, the numerical models were validated for the selected test specimens. Then, fan anchors were added to the models, and their performance in terms of increasing the strength capacity, altering the FRP failure mode, and the strain distribution in the FRP was investigated.

With regard to the application of FRP anchors to FRP strengthened steel structures, two main challenges need to be addressed: a) the connection of FRP dowel to the steel substrate and b) the effectiveness of FRP fan in delaying debonding of FRP from steel. Taking into account the differences between the FRP-steel and FRP-concrete bond-slip behaviour, the issue of local buckling in thin-walled steel members, the complex interaction between post-buckling and debonding modes in FRP-strengthened steel members, along with the fan debonding and rupture as the prevailing failure modes in FRP strengthened concrete structures, reasonably the second question should be answered before overcoming the challenges with the connection of the dowel to the steel. Hence, this study focuses on the effectiveness of fan anchors in strengthening steel structures with the assumption that an adequate connection between the dowel and the steel substrate is provided. In the FE simulations,

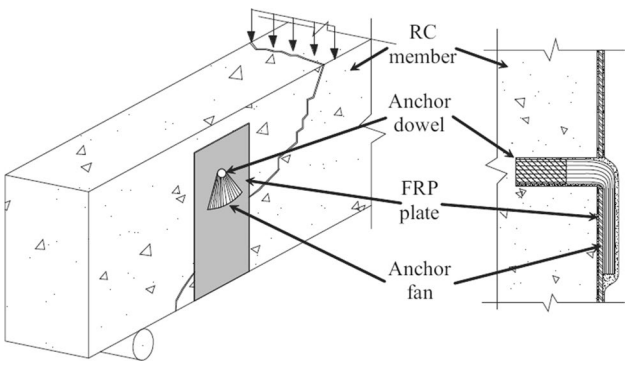

Fig. 1 Schematic display of fan anchor application in FRP-strengthened concrete beam (Zhang et al., 2012)

this assumption was considered by eliminating the dowel part of the fan anchors and restraining its intersection with the fan to the steel member.

2 Numerical Study

Numerical studies were carried out to assess the efficiency of fan anchors in preventing or delaying debonding failure in FRP-strengthened steel structures with different strengthening demands, including enhancing shear, flexural, and buckling performances. First, for each strengthening demand, a Finite Element (FE) model of an experimental test found in the literature was developed and validated using Abaqus FE simulation package. The FRP debonding was the dominant failure mode in all the experimental tests. The FE models were then extended by adding fan anchors to the FRP strengthening system. Finally, the efficiency of the anchorage system was comprehensively assessed by comparing the results of anchored models with that of control specimens (models without fan anchors).

2.1 Fan Anchor Simulation

Fan anchors in FRP-strengthened structures may fail in either of the three following failure modes: fan-to-sheet debonding, fibre rupture, and dowel pull-out (del Rey Castillo et al., 2019). The fibre rupture often occurs at the transition between the fan and dowel. Figure 2 shows the simulation details of a fan anchor.

In this study, it is assumed that the FRP dowel is connected to the steel using an adequate mechanical connection to prevent pull-out failure. The detail of this connection is out of the scope of this study. Hence, to simplify the models, the dowel part was not simulated. Instead, the edge of the fan (at the intersection with the dowel) was fully constrained to a node on the steel surface corresponding to the centroid of the eliminated dowel.

The composite layup option of Abaqus, in conjunction with a local cylindrical coordinate system was adopted to model the fan. The local coordinate system allows fibres to be aligned along the splay. Additionally, the thickness of fan anchors in each study was considered similar to that of the FRP plate in the model.

2.2 Materials Simulation

2.2.1 Adhesive

The adhesive material used to bond the fan to FRP and the FRP to steel substrate was considered in the models to simulate possible debonding. It was assumed that adhesive has elastic behaviour until damage initiates. The onset of damage was determined based on a quadratic stress criterion expressed as

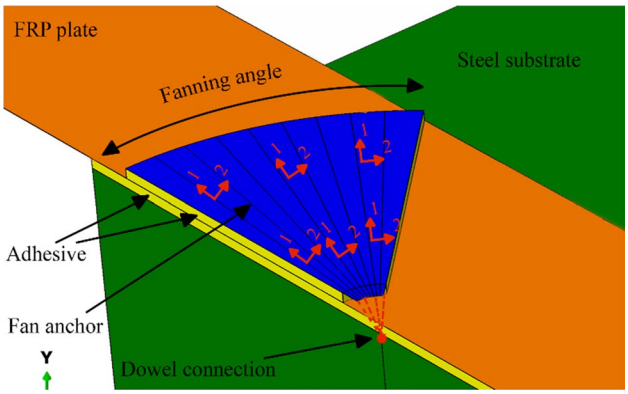

Fig. 2 Details of fan anchor model adopted in Abaqus

$$\left\{\frac{\langle t_n\rangle}{t_n^0}\right\}^2+\left\{\frac{t_s}{t_s^0}\right\}^2+\left\{\frac{t_t}{t_t^0}\right\}^2=1 \tag{1}$$

where t_n, t_s and t_t represent the normal and the two shear tractions, respectively, and t_n^0, t_s^0 and t_t^0 are their corresponding bond strength, respectively.

Propagation of debonding was also tracked using the damage evolution criterion proposed by Benzeggagh and Kenane (1996):

$$G_{IC}+\left(G_{IIC}-G_{IC}\right)\left\{\frac{G_{II}+G_{III}}{G_I+G_{II}}\right\}^{\eta}=G_C \tag{2}$$

In Eq. (2), G_{IC} and G_{IIC} are fracture toughness corresponding to debonding mode I and II, respectively. G_I is the normal strain energy release rate, and G_{II} and G_{III} are the shear strain energy release rate in tangential and transverse directions, respectively. In addition, G_C in Eq. (2) denotes the total mixed-mode fracture energy. In each FE model, the cohesive parameters of adhesive were taken to be identical to those of the adhesive used to bond FRP to steel surface. The cohesive properties of the employed adhesives are given in Tables 1 and 2. In these tables, K_{nn}, K_{ss} and K_{tt} are initial stiffnesses in normal and shear directions, respectively.

2.2.2 CFRP

In the simulation of FRP, elastic behaviour was used in conjunction with the Hashin damage model (Hashin, 1980), which is capable of capturing the FRP rupture. The Hashin theory provides four independent criteria to assess the initiation of fibre tensile failure (F_f^t), fibre compressive failure (F_f^c), matrix

Table 1 Initial cohesive stiffness of adhesives

Model	K_{nn} (N/mm^3)	K_{ss} (N/mm^3)	K_{tt} (N/mm^3)
Single-lap shear (T. Yu et al., 2012)	11,250	667	667
Three-point bending (Dilum Fernando, 2010)	8027	513	513
End bearing loading (Dilum Fernando, 2010)	4812	400	400

Table 2 Cohesive parameters of adhesives

Model	t_n^0(MPa)	t_s^0(MPa)	t_t^0(MPa)	G_{IC} (N/mm)	G_{1IC} (N/mm)	G_{1IIC} (N/mm)
Single-lap shear (T. Yu et al., 2012)	22.34	20.11	20.11	0.041	1.060	1.060
Three-point bending (Dilum Fernando, 2010)	29.70	26.73	26.73	0.0594	1.59	1.59
End bearing loading (Dilum Fernando, 2010)	31.28	28.15	28.15	0.106	7.056	7.056

Table 3 Engineering constants of FRP materials

Model	E_{11} (GPa)	E_{22} (GPa)	ν_{12}	ν_{13}	ν_{23}	G_{12} (GPa)	G_{13} (GPa)	G_{23} (GPa)
Fan anchor (Faggiani & Falzon, 2010)	145	10.3	0.3	0.5	0.495	5.3	5.2	3.9
Single-lap shear (T. Yu et al., 2012)	150	10.3	0.3	0.5	0.495	5.3	5.2	3.9
Three-point bending (Deng & Lee, 2007)	212	10.0	0.3	0.0058	0.0058	3.7	26.5	26.5
End bearing loading (Dilum Fernando, 2010)	300	10.0	0.3	0.0058	0.0058	3.7	26.5	26.5

Table 4 Damage properties of fan anchors (Faggiani & Falzon, 2010)

X_T (MPa)	X_C (MPa)	Y_T (MPa)	Y_C (MPa)	S (MPa)	G_{1C} (N/mm)	G_{1IC} (N/mm)
2000	1600	64	290	98	91.6	1.1

tensile failure (F_m^t) and matrix compressive failure (F_m^c), as follows

$$F_f^t = \left(\frac{\sigma_{11}}{X^T}\right)^2 + \alpha\left(\frac{\sigma_{12}}{S^L}\right)^2 = 1 \tag{3}$$

$$F_f^c = \left(\frac{\sigma_{11}}{X^C}\right)^2 = 1 \tag{4}$$

$$F_m^t = \left(\frac{\sigma_{22}}{Y^T}\right)^2 + \alpha\left(\frac{\sigma_{12}}{S^L}\right)^2 = 1 \tag{5}$$

$$F_m^c = \left(\frac{\sigma_{22}}{2S^T}\right)^2 + \left[\left(\frac{Y^C}{2S^T}\right)^2 - 1\right]\frac{\sigma_{22}}{Y^C} + \left(\frac{\sigma_{12}}{S^L}\right)^2 = 1 \tag{6}$$

In these equations, σ_{ij} denotes the stress tensor's components, X^T and X^C are the fibre's tensile and compressive strengths. Y^T and Y^C refer to the tensile and compressive strengths in the matrix direction. S^L and S^T express the shear strength of FRP in fibre and matrix direction, respectively.

The damage evolution in CFRP was specified on the basis of fracture energy with linear softening. When an element meets one of the above criteria, the corresponding component of the stiffness matrix gradually decreases. The damage level in FRP for each criterion is evaluated by damage parameters varying between 0 and 1, where 0 means no damage and 1 corresponds to complete failure of FRP. The material properties of employed FRP in each model are given in Table 3. The mechanical properties of the fan were adopted from (Faggiani & Falzon, 2010), summarised in Table 4. In this table, G_{IC} and $G_{IIC,}$ are fracture toughness of composite in longitudinal and transverse directions, respectively.

2.2.3 Steel

In all models except the single-lap shear, it was assumed that steel has elastoplastic behaviour with isotropic hardening. In the single-lap shear test model, since the level of strain in the steel plate was considerably lower than yield strain, only the elastic behaviour of the plate was implemented. The mechanical characteristics of steel in each model are presented in Table 5.

2.3 Element Types

In compliance with the Hashin damage model, 4-node general-purpose shell elements with reduced integration (S4R) were employed to model FRP, including the FRP plate and fan. Because of the S4R element's ability to model the features of thin-walled members, this element was also used for simulating the steel components of all models except the first one. The steel plate of the first model was simulated by means of 8-node linear brick elements with reduced integration points (C3D8R).

The adhesive material was simulated using 8-node three-dimensional cohesive element (COH3D8). This element is formulated based on the Cohesive Zone Model (CZM) approach and can predict the possible debonding failure.

3 FE Models, Validation, and Discussion

3.1 Shear Strengthening

The single-lap shear test in (T. Yu et al., 2012) was selected to evaluate the feasibility of fan anchors for the shear strengthening of steel structures. The test setup consisted of a 50 cm FRP plate bonded on a thick steel plate which was fully constrained through welding its bottom to a rigid block. The load was exerted to the unbonded edge of the FRP plate until full debonding of the FRP plate from the steel substrate happened. In accordance with the reported results, most of the specimens failed due to cohesion failure, i.e., failure across adhesive. Among the tested specimens, specimen A-NM-T1 was chosen for simulation. Letter A in the specimen's name indicates the type of adhesive employed. NM stands for normal modulus CFRP, and T1 represents the 1 mm thickness of adhesive. Figure 3(a) shows the modelled specimen and applied boundary conditions. Taking advantage of symmetry, only half of the specimen was simulated. The material properties reported in (T. Yu et al., 2012) were used in the simulation (see Tables 1 and 2). Figure 4 compares the load–displacement curve obtained from the FE simulation, designated A-NM-T1, with the experimental curve, referred to as A-NM-T1-Exp. According to this figure, the numerical model predicted the load–displacement behaviour of the single-lap shear specimen with good accuracy. It is worth mentioning that the slight difference in the initial stiffness of the numerical and the experimental graphs is associated with estimating the displacement at the loaded end of the CFRP plate in the experimental test. This displacement was estimated using the readings of strain gauges bonded on the CFRP plate since the LVDT readings at the loaded end of the CFRP plate were complicated by noise (T. Yu et al., 2012). The numerical model accuracy was also evaluated by comparing the numerical and experimental strain distribution along the length of CFRP. As evident in Fig. 5, the numerical strain distributions at 25% and 89% of the ultimate load are in good agreement with the experimental results.

Following the methodology explained in Sect. 3.1, this model was extended to study the efficiency of fan anchors for shear strengthening by adding one, two, and three anchors at 40 mm intervals (Fig. 3(b)-(d)). The models were named according to the number of employed anchors, e.g., A-NM-T1-1Anc means the model with one fan anchor. The tip of the first fan anchor was located at a 40 mm distance from the left end of the steel plate. The employed fan anchors were 35 mm long with a fanning angle of 90 (see Fig. 2 for the definition of fan angle). To assess the performance of the fan anchors, the results in terms of load–deflection curve, damage propagation, failure mode, and FRP strain profile are presented and discussed below.

3.1.1 Load–Displacement Curve

The load–displacement curves of anchored and unanchored models are compared in Fig. 4. As evident from this figure and also summarised in Table 6, a single row of fan anchors (model A-NM-T1-1Anc) increased the load-carrying capacity (P) by 45% and with the addition of the second anchor (model A-NM-T1-2Anc), this increase reached 66%. However, employing the third fan anchor (model A-NM-T1-3Anc) only enhanced the displacement ductility. Furthermore, using multiple fan anchors resulted in multiple peaks in the load–displacement curves. The occurrence of each peak coincides with the activation and consequent failure of each fan anchor, which is discussed further in Sect. 3.1.3. Accordingly, by FRP debonding reaching the location of

Table 5 Mechanical characteristics of the employed steel

Model	Young modulus (GPa)	Yield stress (MPa)	Tensile strength (MPa)
Single-lap shear (T. Yu et al., 2012)	200	–	–
Three-point bending (Deng & Lee, 2007)	212	329	430
End bearing loading (Flats) (Dilum Fernando, 2010)	192	322	370
End bearing loading (Corners) (Dilum Fernando, 2010)	198	390	450

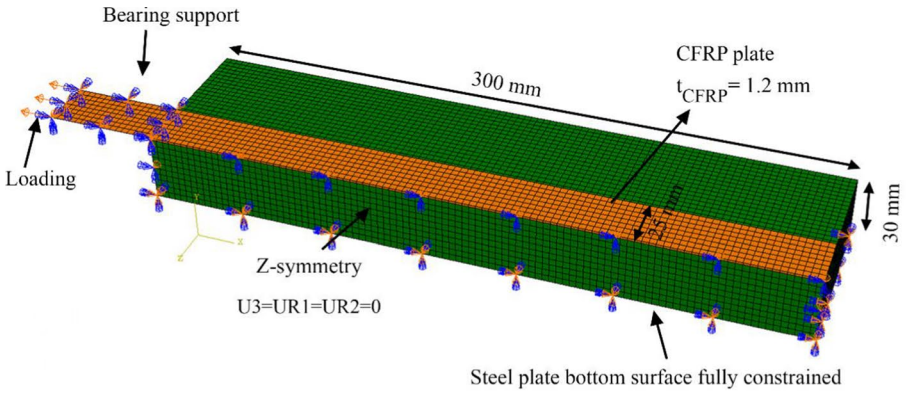

(a)Unanchored model (A-NM-T1)

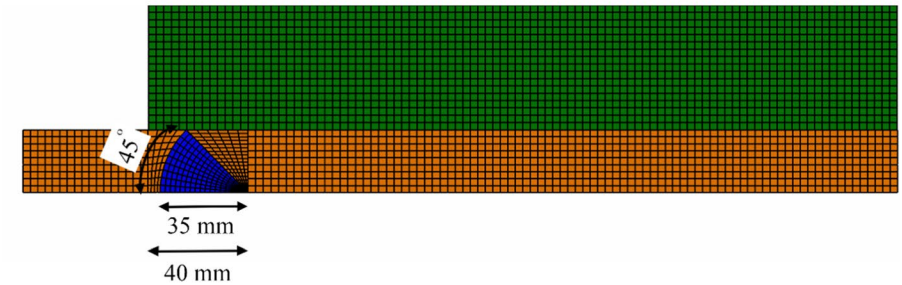

(b)Anchored with 1 fan anchors (A-NM-T1-1Anc)

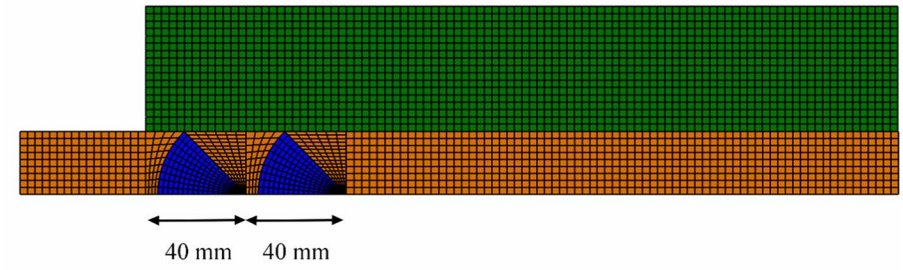

(c)Anchored with 2 fan anchors (A-NM-T1-2Anc)

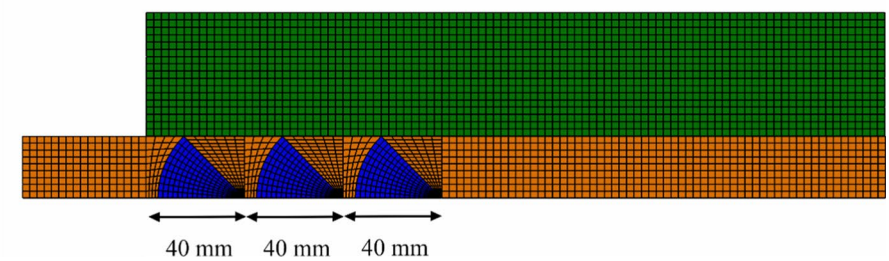

(d)Anchored with 3 fan anchors (A-NM-T1-3Anc)

Fig. 3 FE models of single-lap shear test specimen

the fan anchor, the anchor was activated and started to participate in load bearing, which resulted in the growth of the specimen's strength capacity. However, the attained strength was lost once the anchor failed. Likewise, the activation of the next fan anchor could restore strength to a significant extent. As can be seen in the figure, by the failure of all anchors, the load-carrying capacity of the models was comparable to that of the unanchored specimen. It should be noted that fan anchors did not increase the initial stiffness of the specimens. This is owing to the fact that fan anchors are only activated after the debonding of FRP plate, which itself happens in the nonlinear part of the response.

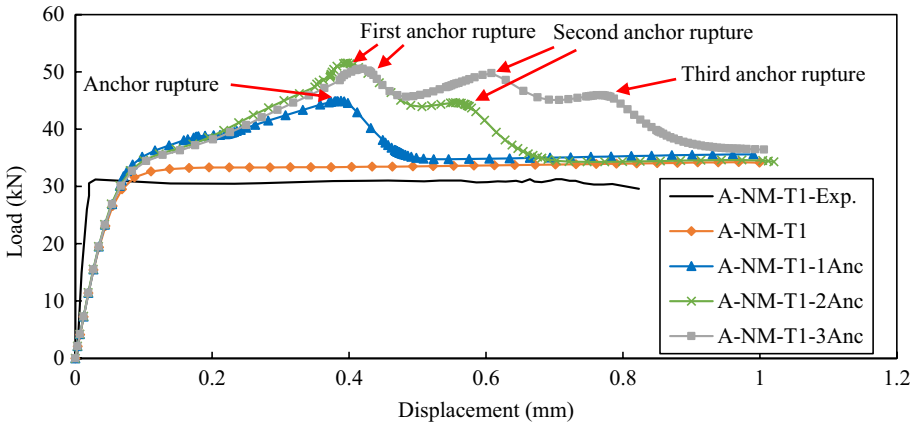

Fig. 4 Load–displacement curves of single-lap shear test models

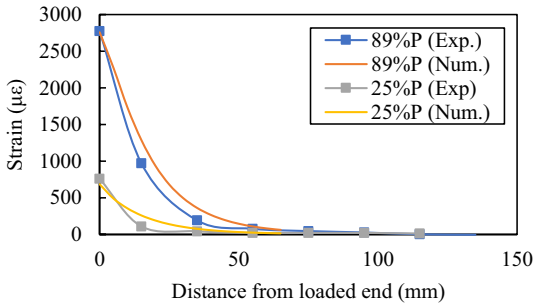

Fig. 5 Comparison of the numerical and the experimental strains along the CFRP plate at 25% and 89% of the ultimate load

Table 6 Key results of shear strengthening study

Model	Number of fan anchors	$\frac{P_{\text{Anchored}}}{P_{\text{Unanchored}}}$ [a]	$\varepsilon_{f,r}(\mu\varepsilon)^b$	$\varepsilon_{f,m}(\mu\varepsilon)^c$	$\frac{\varepsilon_{f,m}}{\varepsilon_{f,r}}$
A-NM-T1	–	–	13,793	3744	0.27
A-NM-T1-1Anc	1	1.45		5656	0.41
A-NM-T1-2Anc	2	1.66		6050	0.62
A-NM-T1-3Anc	3	1.63		6473	0.73

[a] P_{Anchored} and $P_{\text{Unanchored}}$ are the maximum load of anchored and unanchored models, respectively

[b, c] $\varepsilon_{f,r}$ is the rupture strain of the FRP and $\varepsilon_{f,m}$ is the maximum strain in the FRP obtained from FE analysis

3.1.2 Damage Propagation and Failure Mode

Figures 6, 7 and 8 illustrate the debonding status and damage in FRP at different loading stages. To discuss the damage propagation in A-NM-T1-1Anc, A-NM-T1-2Anc, and A-NM-T1-3Anc, four, six, and eight points on the load–displacement curve of each model, respectively, were selected. The first two points represent the load stages corresponding to the onset of debonding and the peak load of the unanchored model (A-NM-T1) and the other points correspond to the peak load and the failure of the anchors or FRP bond.

As shown in Fig. 6, in the case of A-NM-T1 (the model without anchors), following the onset of damage in the adhesive at a load of 26.5 kN (point 1), sudden debonding progress in the adhesive layer restricted the peak load to 33.3 kN (point 2). As explained previously and presented in Fig. 7, the load-carrying capacity of A-NM-T1-1Anc exceeds point 2 (33.3 kN) as a result of the anchor's activation. This increase continued until the peak load at point 3 (44.9 kN), where the damage in the fan at the intersection with the dowel was initiated, see Fig. 7(b). At this point, the model experienced strength degradation until its load-carrying capacity decreased to 35.17 kN (point 4), a load level comparable with the peak of the unanchored model (A-NM-T1).

A similar scenario can be observed in A-NM-T1-2Anc where the damage initiation of the first anchor (the anchor closer to the loaded end of the FRP plate) at peak load corresponding to 51.5 kN (point 3) was followed by a relatively sharp load decay until point 4 (43.91 kN). Next, the load-carrying capacity showed a negligible increase up to 44.6 kN (point 5). However, the onset of the damage in the second fan and its progress lowered the model's load-carrying capacity up to a strength comparable to that of the unanchored specimen (point 6).

Similarly to the other anchored models, the failure of the A-NM-T1-3Anc was due to the rupture of all three pairs of fan anchors at their intersection with the dowel (Fig. 9). In this specimen, the failure started from the closest pair of anchors to the loaded end of the FRP plate followed by the failure of the second and third pairs of anchors. By the failure of the last pair of fan anchors, the load-carrying capacity decreased to 37.78 kN (point 8), nearly the load-carrying capacity of the unanchored specimen.

The comparison of the debonding progress (status) in the FRP plate of the unanchored and anchored models at point 2 reveals that while a certain length of FRP was fully

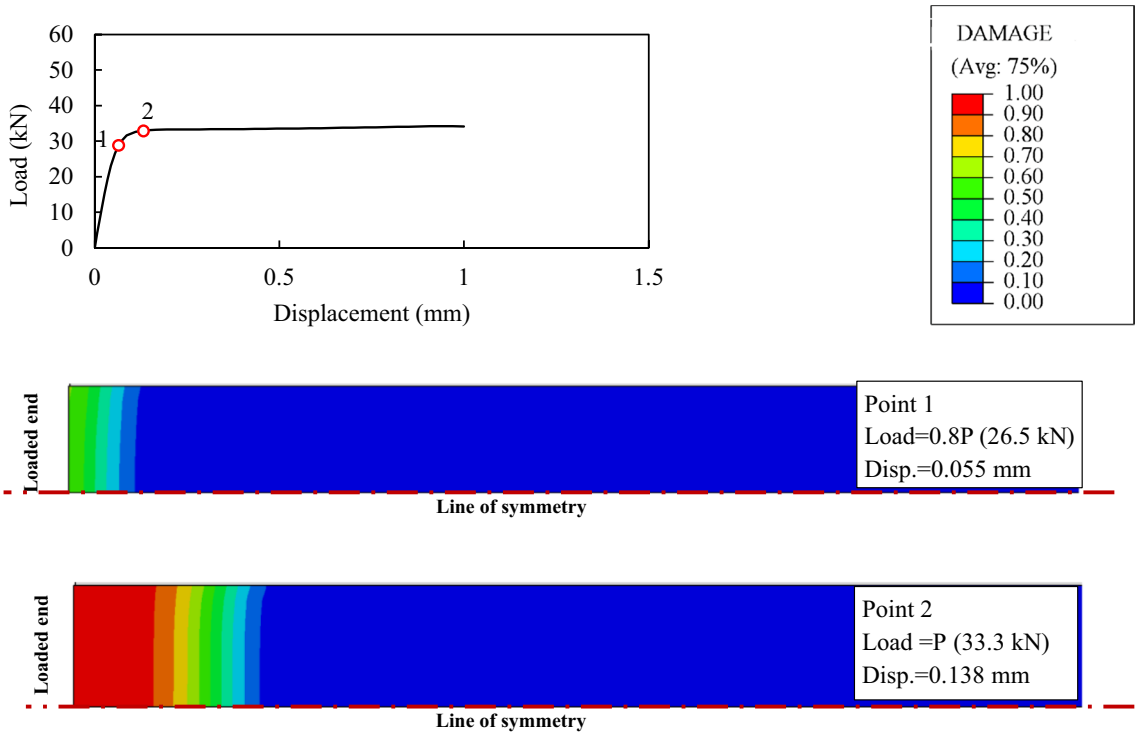

Fig. 6 Debonding status in adhesive layer at different loading stages (A-NM-T1)

debonded in A-NM-T1, the debonding had not yet started in the anchored models, demonstrating the efficiency of fan anchors at precluding damage propagation.

3.1.3 FRP Strain Profile

The premature debonding of FRP plate from structures prevents exploiting its full strengthening capacity (American Concrete Institute (ACI), 2017). Adequate anchorage systems, however, can retrieve FRP tensile capacity by postponing premature debonding (Yazdani et al., 2020). The performance of fan anchors at retrieving FRP capacity was evaluated through assessing the strain profile of FRP plate.

The strain profile along the centreline of the FRP plate and fan anchors was extracted at different loading stages and plotted in Figs. 10, 11, 12 and 13 for each model. As can be seen in these figures, before the onset of debonding (point2), the strain in the FRP plate for all models is similar. However, after debonding initiation, the fan anchors contributed to the strain distribution, and higher strain levels developed in the anchored models. In addition, despite a uniform strain profile in the unanchored model, high strain concentrations at the locations of the fan anchors can be observed in the other models.

In order to evaluate the activation and contribution of the fan anchors through debonding of the FRP plate, the strain distribution along each fan is discussed here. Before the debonding initiation, i.e., point 1 and point 2, only a negligible strain was developed in the fan anchors, indicating that fan anchors had not been activated yet. Nonetheless, at the maximum load (point3), the tip of the first fan anchor reached the FRP's rupture strain indicating that the first anchor had been activated somewhere between point 2 and point 3 (Fig. 11b). The strain level in the second anchor of A-NM-T1-2Anc and A-NM-T1-3Anc models at point 3 also demonstrates activation of this anchor (see Figs. 12b and 11b). However, at the same load stage (point 3), the strain in the third anchor is still insignificant (see Fig. 13b). At the second peak (point 5), the strain in the second fan of both A-NM-T1-2Anc and A-N-MT10-3Anc models reached the FRP's rupture strain which resulted in the activation of the third anchor in A-N-MT10-3Anc. Finally, at point 7, the third anchor of A-NM-T1-3Anc reached its rupture strain. The damage propagated through the anchor's fan until it failed at point 8. Hence, taking into account the strain level of fan anchors at different loading stages, it can be concluded that the activation and failure of each fan anchor were correlated with the debonding status in the FRP plate.

For each model, the maximum strain in the FRP plate ($\varepsilon_{f,m}$) was extracted and compared in Table 6. Strain efficiency in each model was evaluated based on the ratio of the $\varepsilon_{f,m}$ to the rupture strain ($\varepsilon_{f,r}$). As indicated in this table,

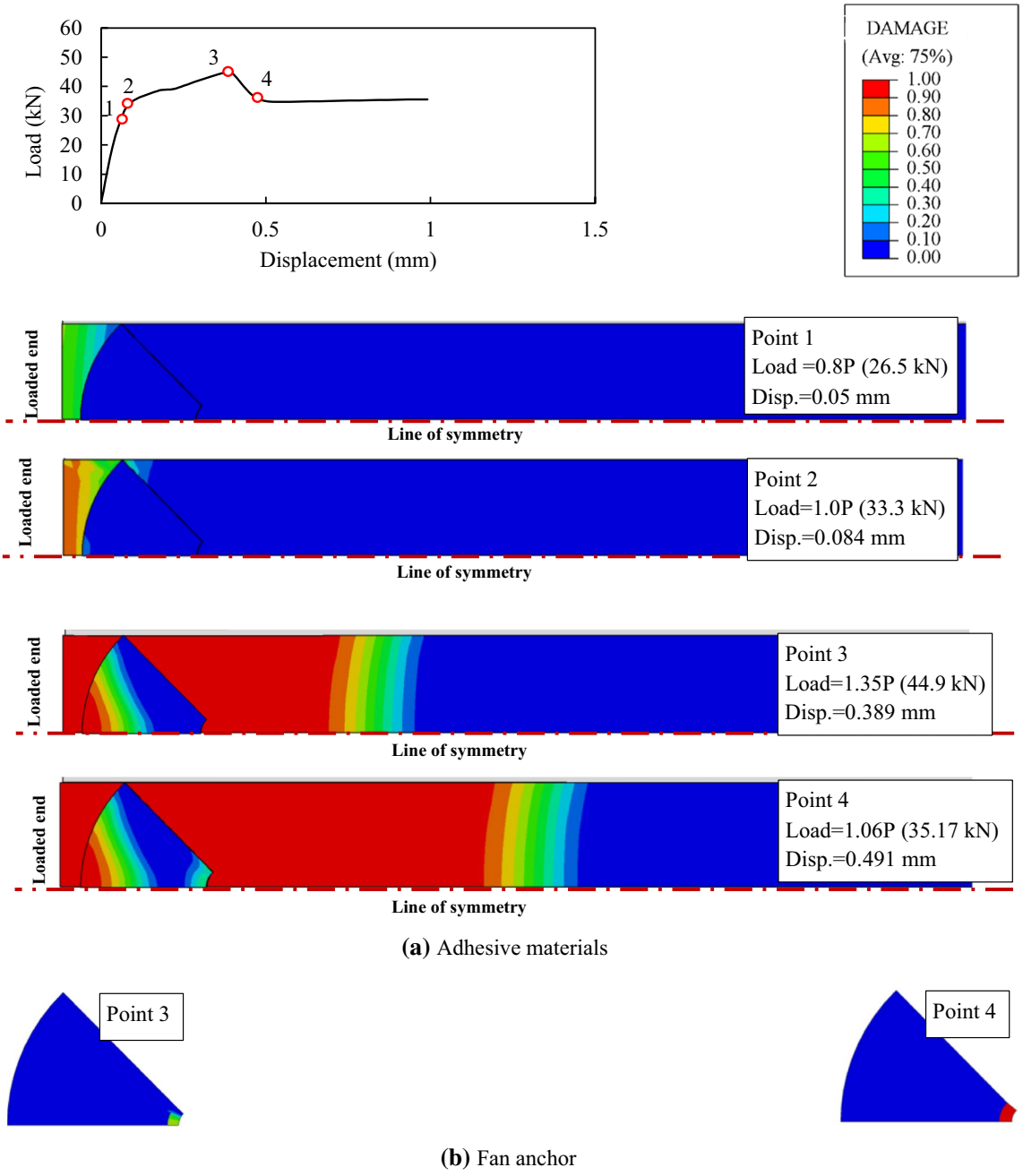

Fig. 7 Debonding and damage status at different loading stages (A-NM-T1-2Anc)

whilst the maximum FRP strain in the unanchored model is only 27% of the FRP's rupture strain, installing one, two and three anchors increased this ratio to 41%, 62% and 73%, respectively. This indicates the efficiency of fan anchors in improving FRP's maximum strain, hence better use of the material capacity.

3.2 Flexural Strengthening

As a second example, the efficiency of the fan anchors was examined for flexurally strengthened steel structures failing by FRP debonding. As demonstrated by previous studies (Deng et al., 2004; Schnerch et al., 2007), plate-end detachment in flexurally strengthened elements is due to mixed mode I-mode II debonding. Hence, the efficiency of fan anchors to prevent/delay the mixed-mode debonding is explored by simulating one of the FRP-strengthened

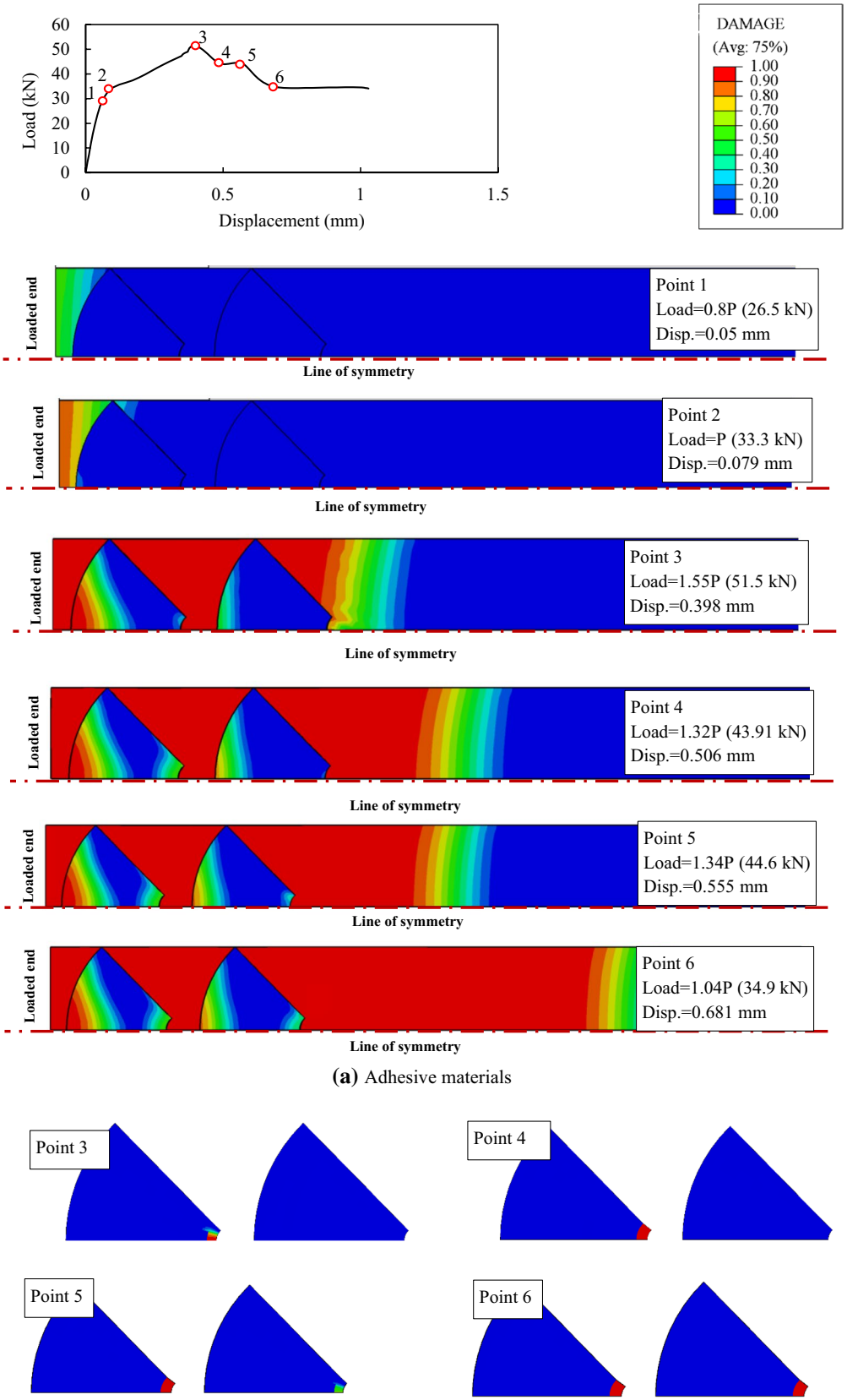

(a) Adhesive materials

(b) Fan anchors

Fig. 8 Debonding and damage status at different loading stages (A-NM-T1-2Anc)

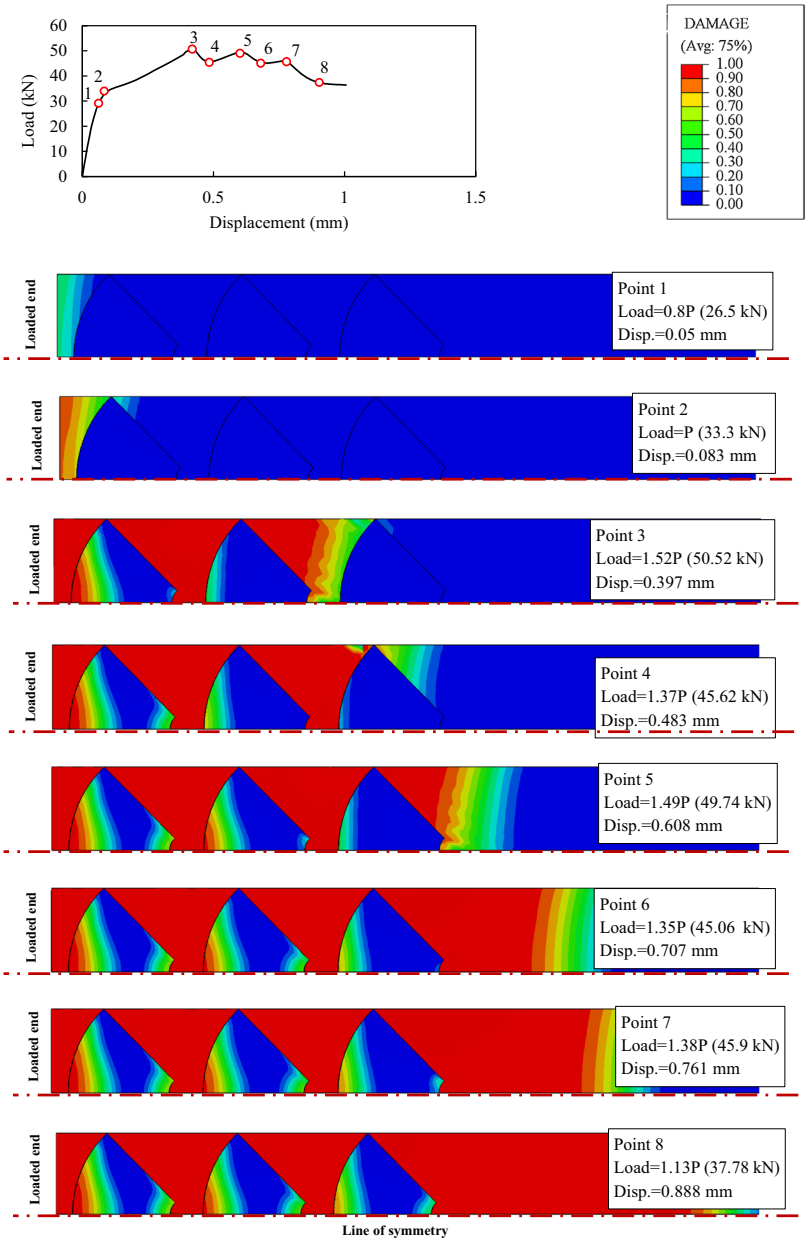

(a) Adhesive materials

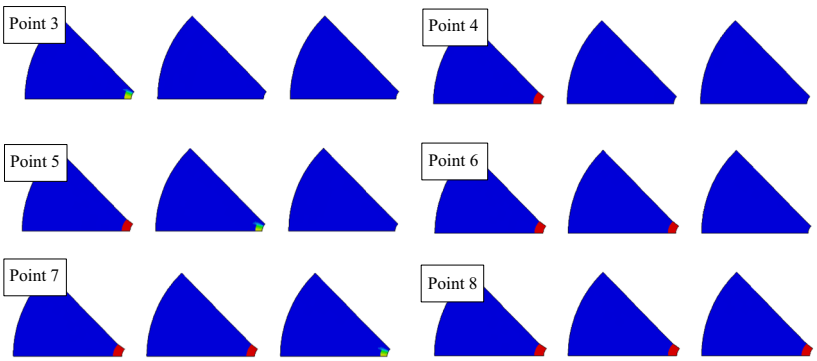

(b) Fan anchors

Fig. 9 Debonding and damage status at different loading stages (A-NM-T1-3Anc)

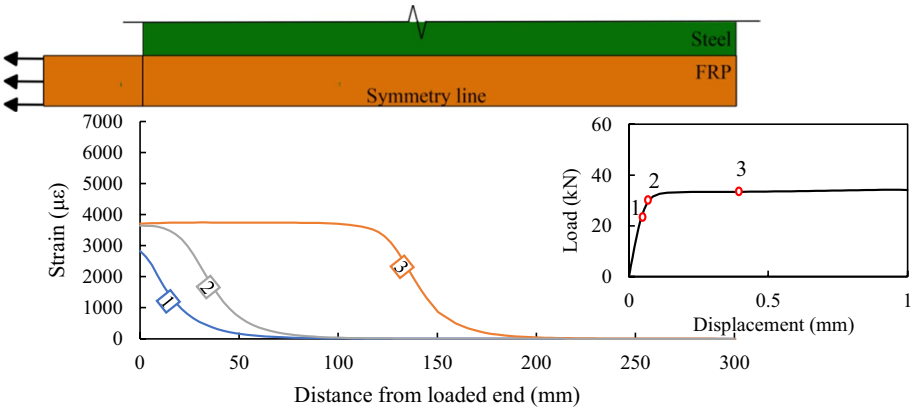

Fig. 10 Strain distribution along FRP at different loading stages (A-NM-T1)

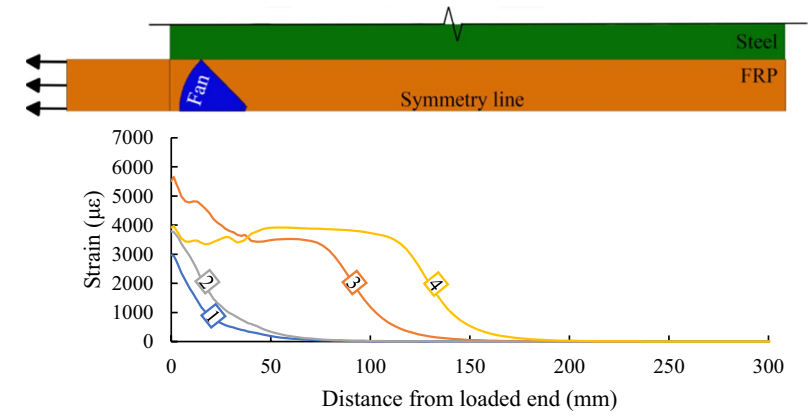

(a) FRP plate

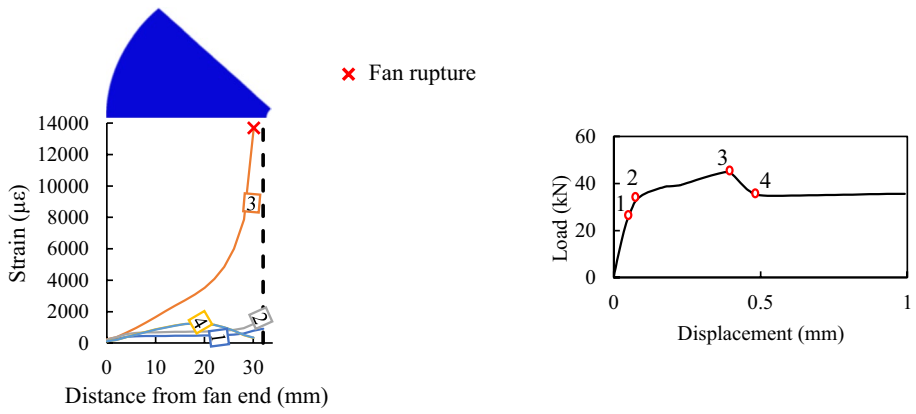

(b) Fan anchor

Fig. 11 Strain distribution along FRP at different loading stages (A-NM-T1-1Anc)

steel I-beams tested by Deng and Lee (2007). The selected specimen was named S303, in which the first 3 indicates a 3-point bending test and the last two digits refer to the length of CFRP equal to 0.3 m. Specimen S303 was a 1.1 m long beam with a cross-section of 127 × 76UB13, which was strengthened through bonding a 3 mm thick CFRP plate to the bottom flange of the beam. The CFRP plate had a length of 300 mm and bonded to the mid-span of the beam using Sikadur-31 Normal. The properties of the materials are given in Tables 1, 2, 3 and 5. The specimen was tested under three-point bending loading and failed due to CFRP plate debonding. The FE model of the specimen is presented in Fig. 14. Taking advantage of double symmetry only a quarter of the specimen was simulated. Uniformly fine mesh was adopted for the FRP-strengthened length of the model which was then gradually enlarged by getting farther from the strengthened region.

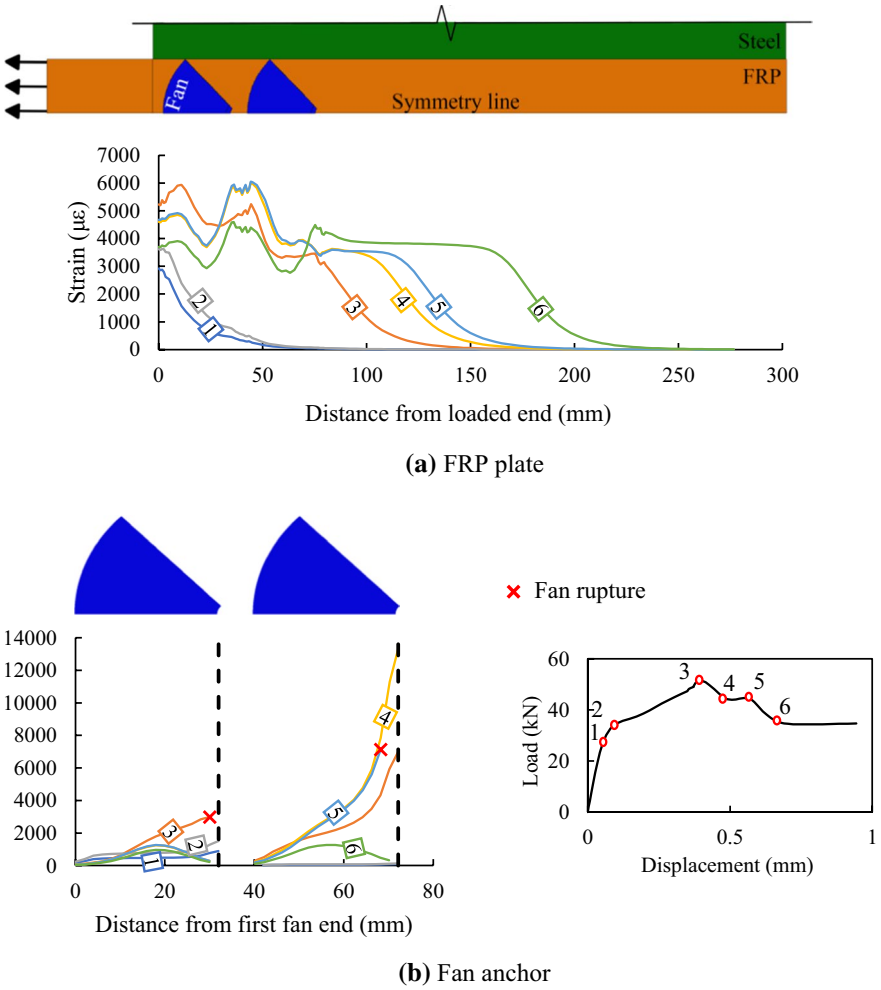

Fig. 12 Strain distribution along FRP at different loading stages (A-NM-T1-2Anc)

(a) FRP plate

(b) Fan anchor

As illustrated in Fig. 16, the load–deflection curve obtained from the numerical simulation (S303) is in good agreement with that of the experimental test (S303-Exp). Moreover, similarly to experimental observation, debonding was initiated from the ends of the FRP plate. This validated model was upgraded by adding one, two and three rows of fan anchors. Each row was composed of a pair of anchors installed symmetrically with respect to the beam's longitudinal plane of symmetry. These models were designated S303-1Anc, S303-2Anc and S303-3Anc, respectively, and are detailed in Fig. 15. In the S303-1Anc model, a pair of anchors, each with a length of 27 mm and a fanning angle of 90°, was employed to the end of FRP plate (Fig. 15b). In S303-2Anc and S303-3Anc models, two and three pairs of similar fan anchors were used at 29 mm intervals (Fig. 15c and d), respectively.

3.2.1 Load–Displacement Curve

Figure 16 plots the load–deflection response of unanchored and anchored models. Adding fan anchors had a negligible influence on initial stiffness but increased the ultimate strength to some extent. One of the parameters to describe the capability of a structural member to withstand large deformations is ductility, μ, defined as

$$\mu = \frac{\Delta_u}{\Delta_y} \tag{7}$$

where Δ_u and Δ_y are the ultimate and yield displacements of the beam and obtained from the load–displacement curve using park's definition (Park, 1989). Accordingly, yield displacement corresponds to a displacement that yielding initiates, and ultimate displacement corresponds to a displacement that load-bearing capacity is reduced by 20%. As presented in Table 7, installing one pair and two pairs of fan anchors increased the beam's ductility by 33% and 64%, respectively. Thus, despite the slight increase in the maximum load, fan anchors notably increased flexural ductility.

As in the case of the previous example, activation and failure of the fan anchors are manifested as crests in the load–deflection curves. Comparing the results of the

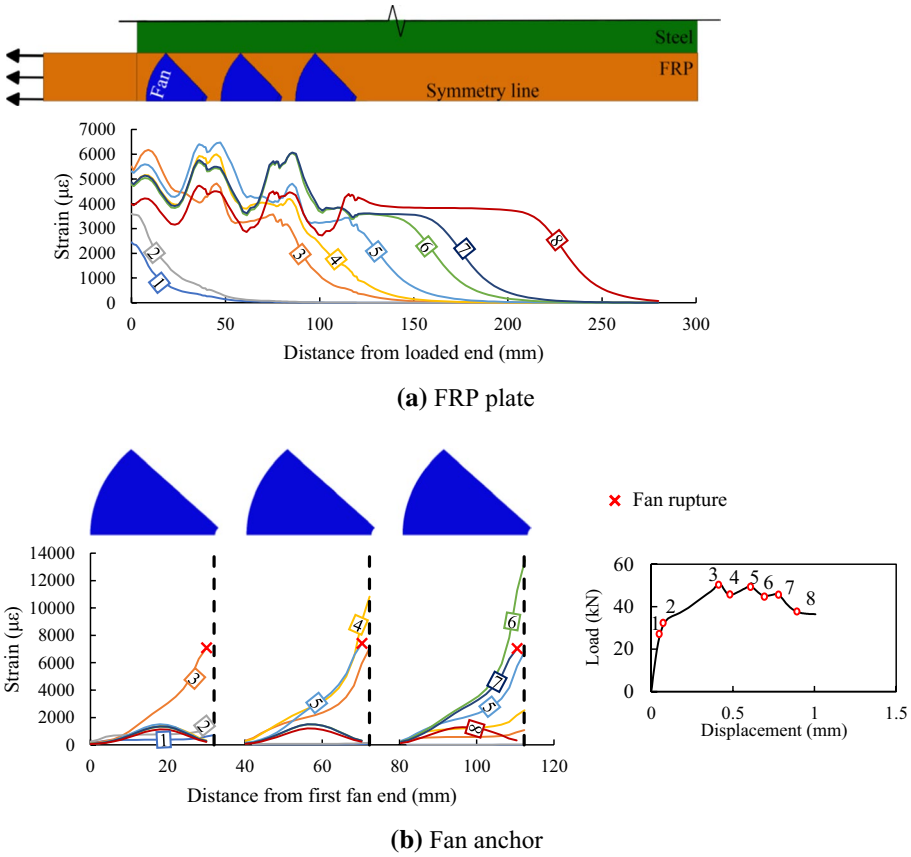

Fig. 13 Strain distribution along FRP at different loading stages (A-NM-T1-3Anc)

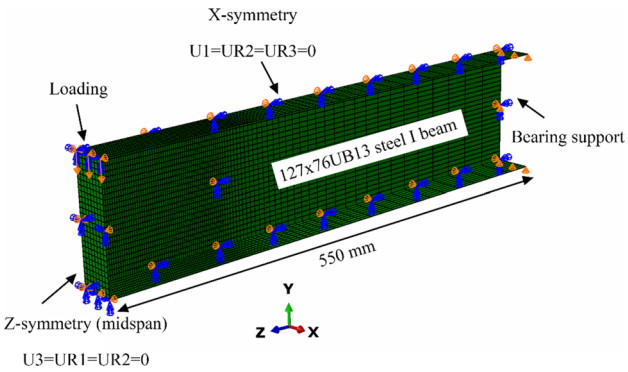

Fig. 14 Finite element model of FRP-strengthened steel I-beam (a quarter specimen was modelled due to double symmetry)

S303-2Anc and S303-3Anc in Table 7 reveals that using the third pair of anchors was ineffective in increasing the beam's ductility or strength. The third pair of anchors are almost entirely located out of the anchorage length of the CFRP plate; hence, their ineffectiveness in preventing the plate-end debonding. The anchorage length is the length of the FRP extended beyond the theoretical termination point, the point beyond which the strengthened beam's flexural demand is lower than the moment capacity of the bare beam.

The bending moment diagram of the beam S303-3Anc at the peak load, along with the flexural capacity of the bare steel section, M_{un} (the horizontal dashed line), is shown in Fig. 17. According to this figure, at the peak load of the beam S303-3Anc, the anchorage length of CFRP is 61 mm. While the first 2 pairs of anchors are entirely located within the anchorage zone, the third pair of anchors are almost entirely positioned outside this zone.

3.2.2 Failure Mode

The damage status in FRP and adhesive materials and the status of plastic strain in steel at the failure load are depicted in Figs. 18, 19 and 20 for each model. According to these Figures, the fan anchors did not alter the FRP plate-end debonding failure mode, which was the case in the unanchored beam. In all models, the fan anchors failed by debonding from the FRP plate with only negligible damage to the fan part of the anchors (Figs. 18c, 19 and 20c). In addition, the comparison of Fig. 18a and 20a shows that utilising fan anchors induced plastic strain concentration in the bottom flange and lower part of the web, and by increasing the number of anchors, plastic strain is more distributed in these areas.

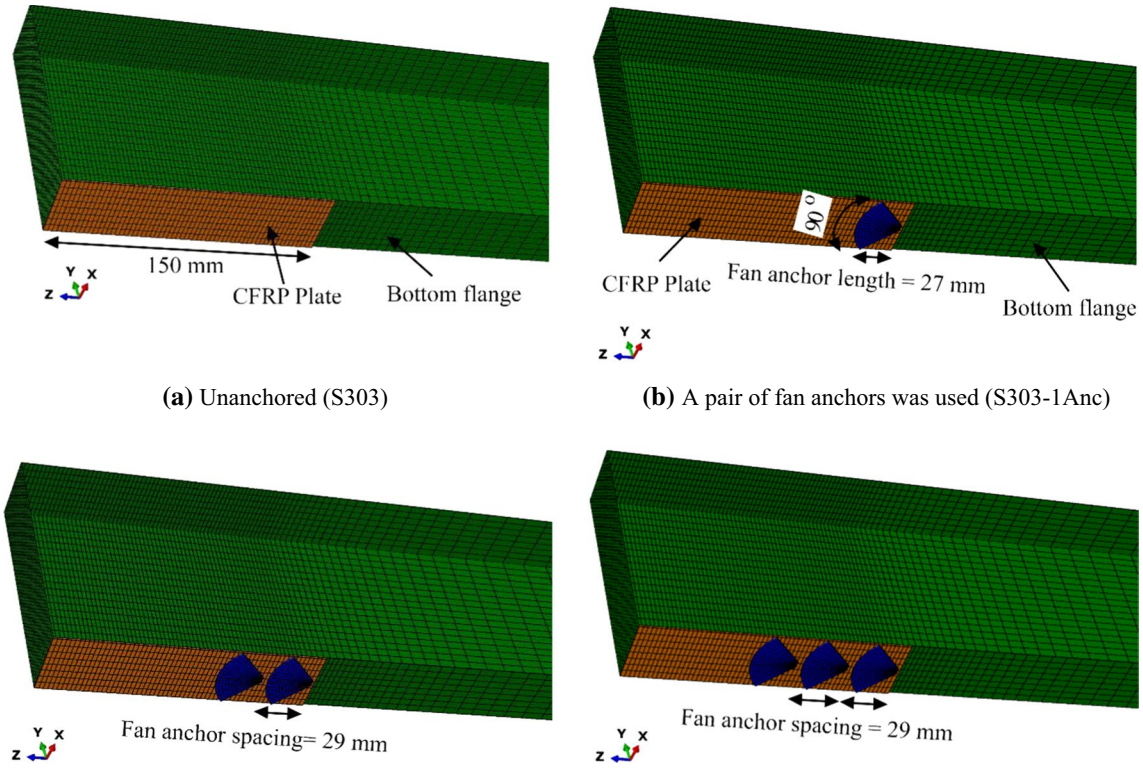

(a) Unanchored (S303)

(b) A pair of fan anchors was used (S303-1Anc)

(c) 2 pairs of fan anchors were used (S303-2Anc)

(d) 3 pairs of anchors were used (S303-3Anc)

Fig. 15 FE models of three-point bending test specimens

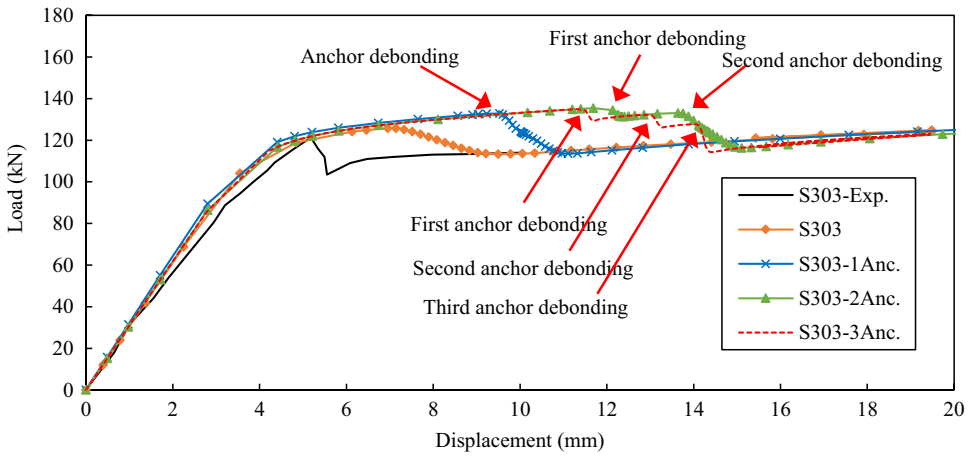

Fig. 16 Load–displacement curves of anchored and unanchored FRP-strengthened beams

Table 7 Key results of flexural strengthening study

Model	Number of fan anchors	$\frac{P_{\text{Anchored}}}{P_{\text{Unanchored}}}^{a}$	Ductility	$\varepsilon_{f,r}(\mu\varepsilon)^{b}$	$\varepsilon_{f,m}(\mu\varepsilon)^{c}$	$\frac{\varepsilon_{f,m}}{\varepsilon_{f,r}}$
S303	–	–	2.02	16,038	3243	0.20
S303-1Anc	2	1.09	2.69	16,038	3907	0.24
S303-2Anc	4	1.08	3.30	16,038	4444	0.28
S303-3Anc	6	1.07	3.20	16,038	4278	0.27

[a, b, c] See Table 6 for definition of the notations

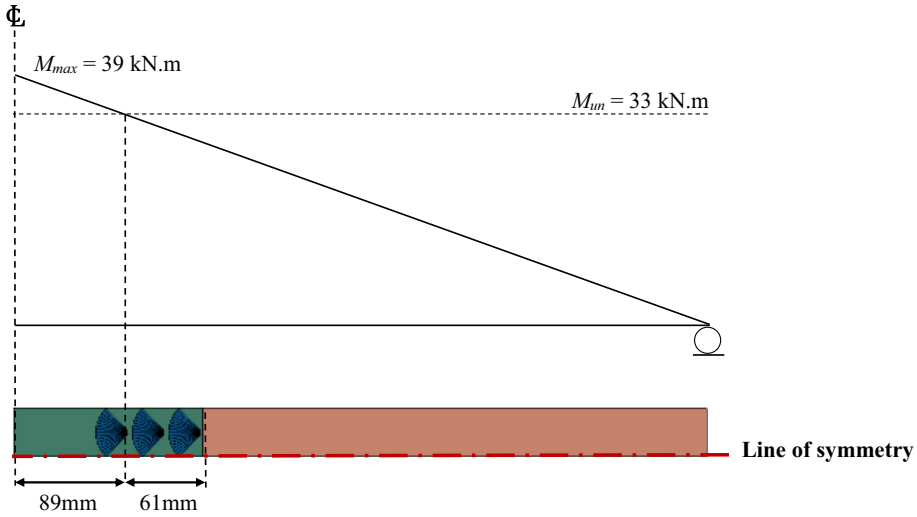

Fig. 17 The bending moment diagram of S303-3Anc at the peak load. The horizontal dashed line corresponds to the moment capacity of the unstrengthened (bare) beam

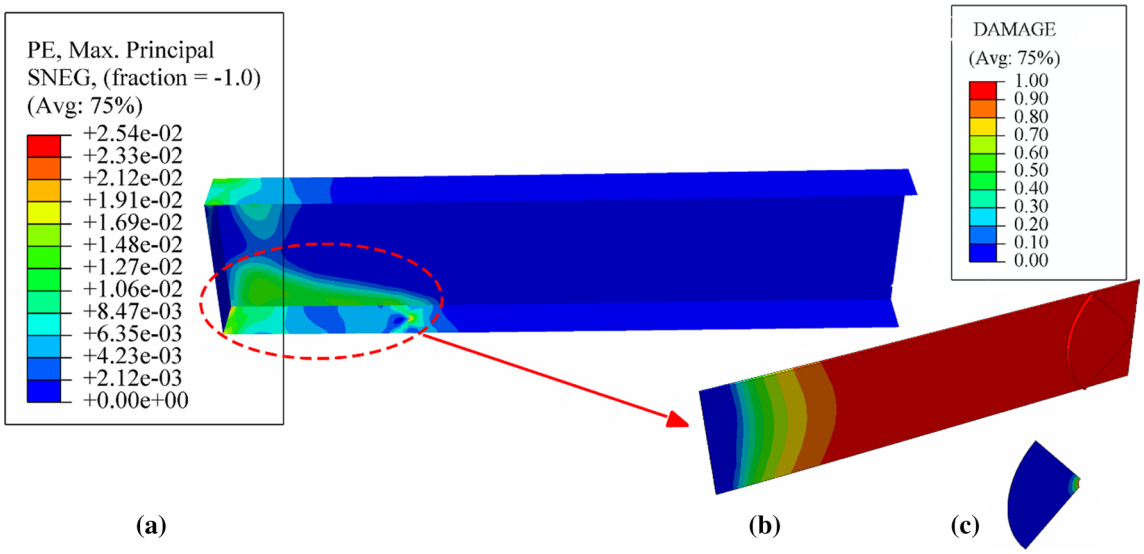

Fig. 18 Specimen S303-1Anc at the failure stage: **a** Plastic strain (PE) in the I-beam, **b** damage status in the adhesive, and **c** damage status in the fan anchors

3.2.3 FRP Strain Profile

Similarly to the previous example, the effect of fan anchors on improving the maximum strain developed in FRP plate is explored. Figures 21, 22, 23 and 24 present the axial strain distribution along the plate's centreline at different loading stages. The first two loading stages, point 1 and point 2, stand for the onset of debonding and the peak load of the unanchored model (S303), respectively. The remaining points correspond to peak load, fan anchor failure, and FRP debonding. In these figures, the zero strain indicates FRP debonding from the steel. From the strain profiles, it can be seen that while the FRP plate in S303 was fully debonded at a deflection of 11 mm (point 4), fan anchors enabled FRP to further contribute to the load-carrying mechanism by delaying the FRP detachment. At 15 mm deflection, despite the complete FRP detachment in S303-1Anc, only a limited debonding occurred in S303-2Anc, indicating that an additional pair of fan anchors successfully deferred the FRP detachment.

According to the strain efficiency $\left(\varepsilon_{f,m}/\varepsilon_{f,r}\right)$ given in the last column of Table 7, adding the first and second row(s) of fan anchors in S303-1Anc and S303-2Anc models raised strain efficiency from 20 to 24% and 28%, respectively.

3.3 Buckling Strengthening

To assess the efficiency of fan anchors in buckling failure, the end bearing tests in (Dilum Fernando, 2010) was selected. Through experimental and numerical studies,

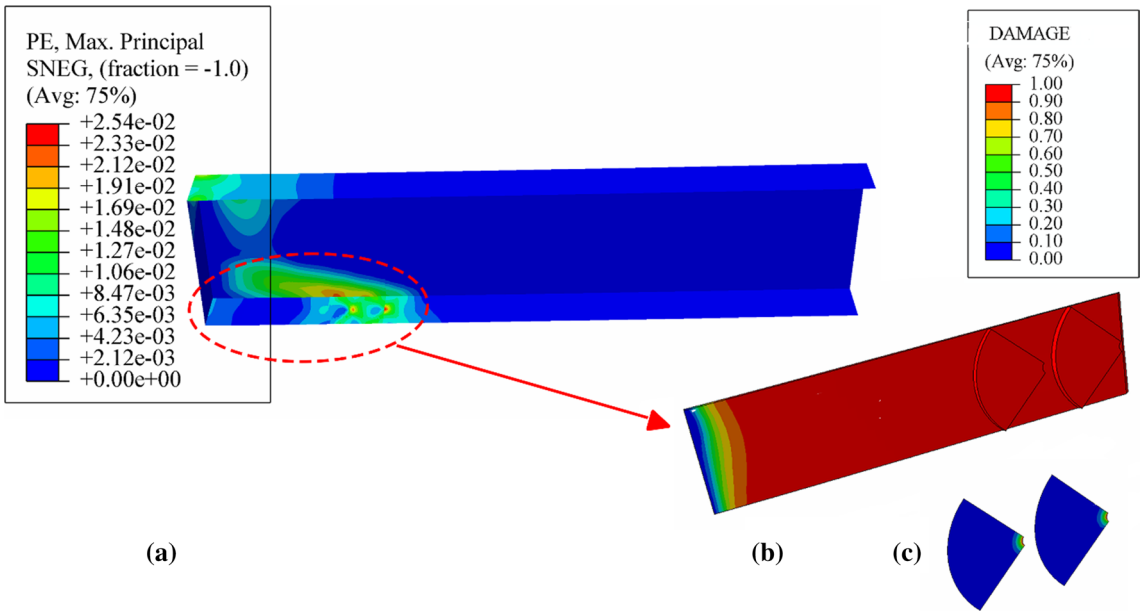

Fig. 19 Specimen S303-2Anc at the failure stage: **a** Plastic strain (PE) in the I-beam, **b** damage status in the adhesive, and **c** damage status in the fan anchors

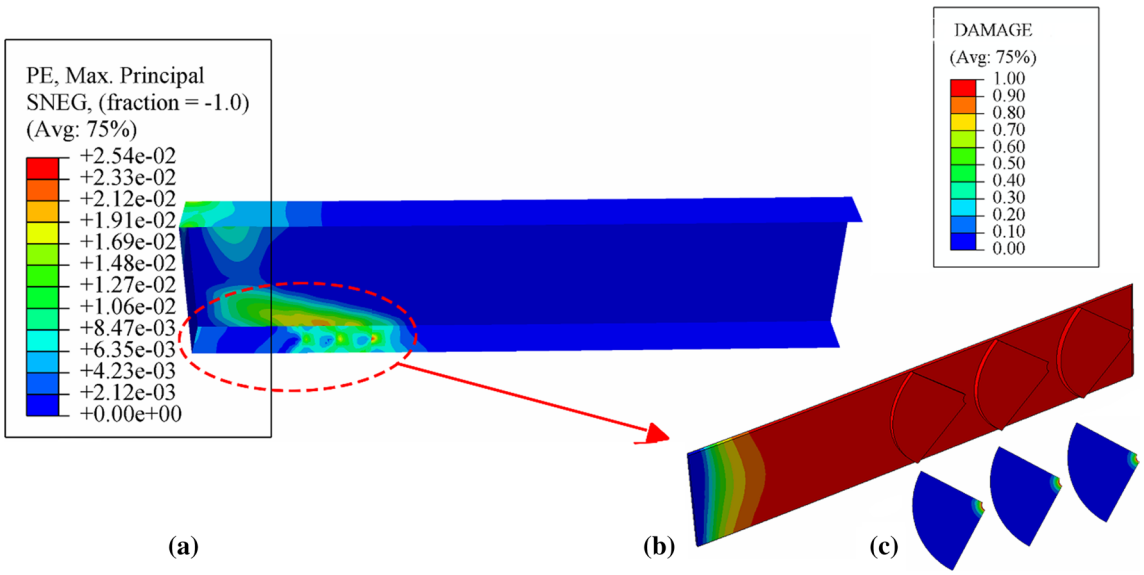

Fig. 20 Specimen S303-3Anc at the failure stage: **a** Plastic strain (PE) in the I-beam, **b** damage status in the adhesive, and **c** damage status in the fan anchors

Fernando et al. (2010) examined the applicability of FRP plate for enhancing the web crippling of Rectangular Hollow Section (RHS) tubes which is a typical failure mode among thin-walled structures under transverse load. They strengthened a set of RHS tubes using different types of adhesives and FRP patterns. Then, specimens were placed on a rigid steel plate, and an incremental compressive displacement was applied to their upper flange until failure. According to their study, the FRP plate substantially improves the load-bearing capacity of the RHS tubes. The strengthening system nevertheless failed due to FRP premature debonding. In the current study, fan anchors are employed to evaluate their efficiency at delaying debonding under large deformation conditions. Among tested specimens, specimen S30-A was simulated. S30 in the specimen's designation refers to the adhesive type Sika

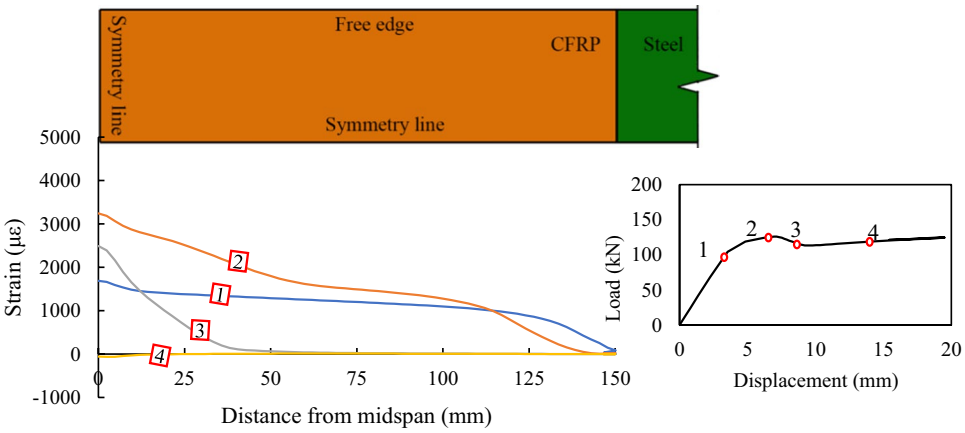

Fig. 21 FRP strain distribution in S303 at different loading stages up to debonding

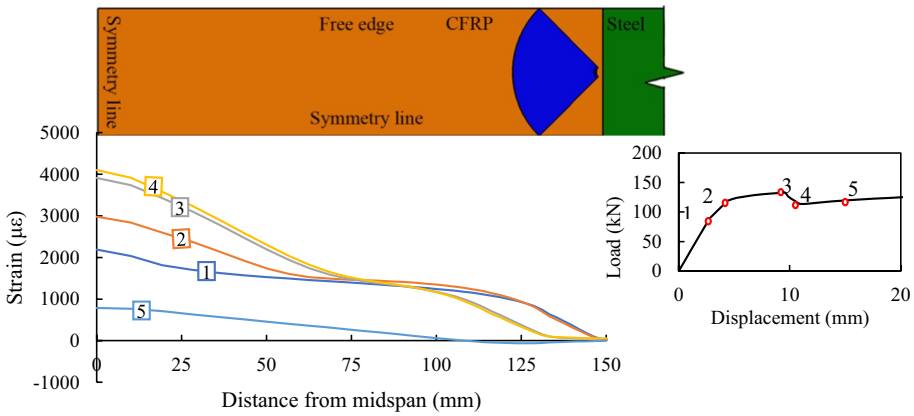

Fig. 22 FRP strain distribution in S303-1Anc at different loading stages up to debonding

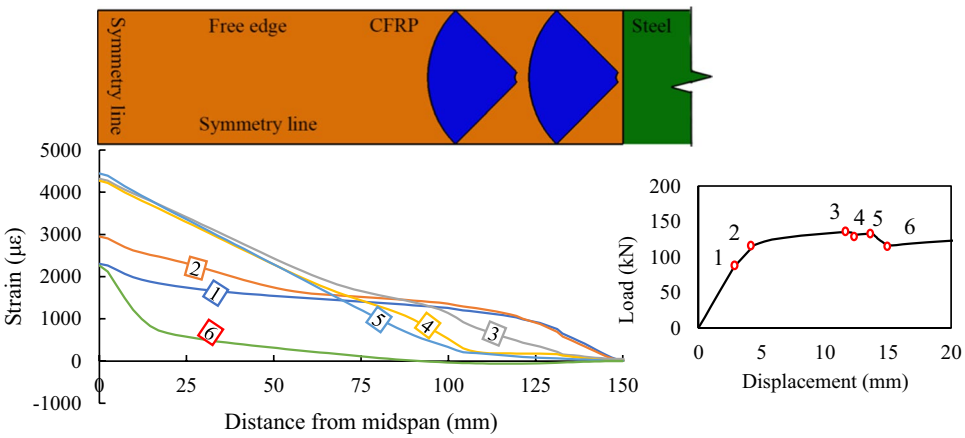

Fig. 23 FRP strain distribution in S303-2Anc at different loading stages up to debonding

30, and A denotes the section type, namely 100–5-2 RHS tube. This specimen was strengthened by bonding two CFRP plates, with fibres along the vertical direction, to the external surface of its webs. The numerical model and the applied boundary conditions are presented in Fig. 25. Taking advantage of symmetry, only half of the specimen was modelled. In addition, the loading plate and the baseplate were included in the simulation and assumed to be rigid.

3.3.1 Load–Displacement Curve

Figure 26 compares the load–displacement curve attained from the numerical simulation (S30-A) against that of the experimental test (S30-A-Exp) in (Dilum Fernando, 2010). According to this figure, a good agreement between the numerical and experimental curves can be identified.

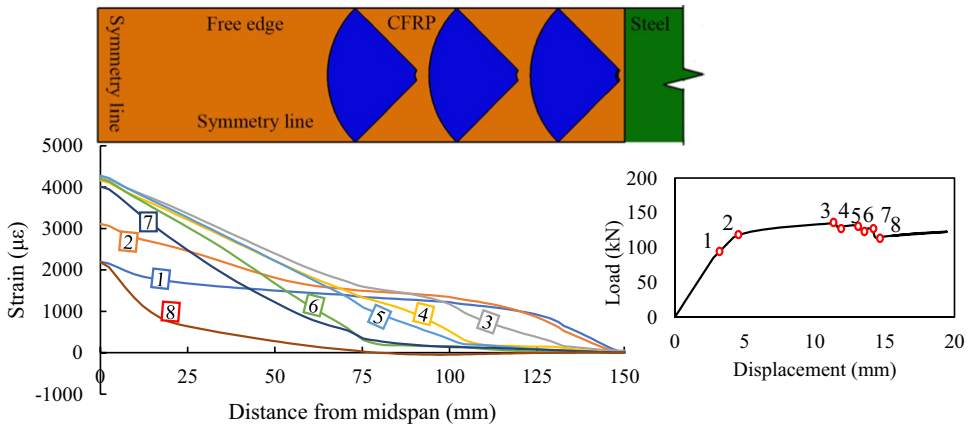

Fig. 24 FRP strain distribution in S303-3Anc at different loading stages up to debonding

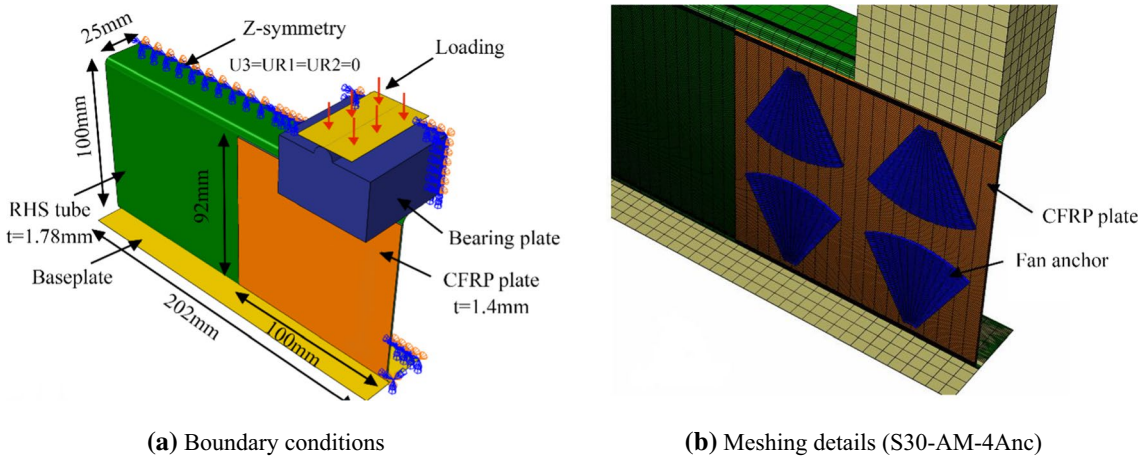

(a) Boundary conditions **(b)** Meshing details (S30-AM-4Anc)

Fig. 25 Graphical representation of FE models developed for end bearing load specimens

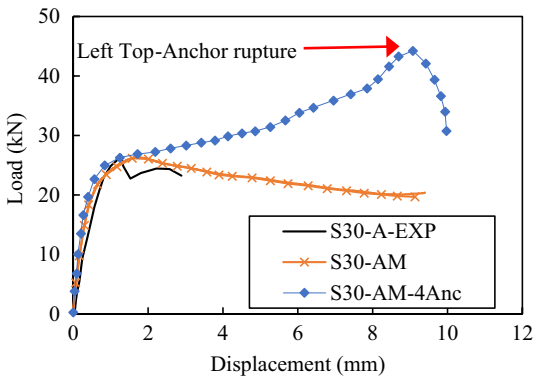

Fig. 26 Load–displacement curves of end-bearing models

The validated FE model was extended by adding two rows of 40 mm long fan anchors having a fanning angle of 60° and designated S30-AM-4Anc. The fan anchors were distributed symmetrically with respect to the central axes of the FRP plate. The dowel of fan anchors was assumed to be close to the horizontal edge of the CFRP plate with a 25 mm distance from the vertical edge. The arrangement of fan anchors is presented in Fig. 27.

In the anchored FRP-strengthened RHS models, the FRP plate was prone to rupture due to a high strain concentration at the location of the fan anchors. Since the parameters required to simulate the damage initiation and evolution in the FRP plate were not reported in (Dilum Fernando, 2010), the material properties of the FRP plate were taken identical to those of fan anchors (See Table 4) to allow for capturing any possible FRP failure.

The load–deflection response of the unanchored and the anchored models are compared in Fig. 26. Adding fan anchors had a negligible influence on the initial stiffness; nevertheless, they resulted in a notable increase of 68% in the load-bearing capacity of the FRP-strengthened RHS tube (See Table 8). Contrary to previous examples, by utilising two rows of anchors, only one crest appeared in the load–displacement curve of S30-AM-4Anc. This can be explained

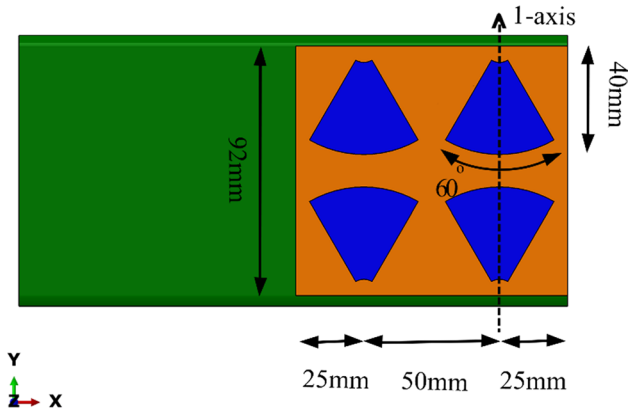

Fig. 27 Fan anchors arrangement in S30-AM-4Anc model

Table 8 Key results of the buckling strengthening study

Model	Number of fan anchors	$\frac{P_{\text{Anchored}}}{P_{\text{Unanchored}}}^{a}$	$\varepsilon_{f,r}(\mu\varepsilon)^{b}$	$\varepsilon_{f,m}(\mu\varepsilon)^{c}$	$\frac{\varepsilon_{f,m}}{\varepsilon_{f,r}}$
S30-AM	–	–	13,793	3744	0.27
S30-AM-4Anc	4	1.68		13,793	1

[a, b, c] See Table 6 for the definition of the notations

by the fact that debonding initiated and propagated from the top right corner of the FRP plate, which activated only one of the anchors.

3.3.2 Failure Mode

Figures 28 and 29 show the plastic strain status in the steel box and the damage status in the FRP and the adhesive at failure. A symmetric configuration of fan anchors, did not modify the location of debonding. Debonding propagated through the top right corner of the FRP plate in both anchored and unanchored models. Then, only the top right fan anchor failed. As displayed in Fig. 29, the anchor failure was governed by fan rupture accompanied by partial debonding at its connection to the dowel. Some minor damages can also be observed in other fan anchors. Furthermore, the FRP plate ruptured at the fan anchor's connection to the steel substrate, whereas no damage was seen in the FRP plate of the S30-AM model. It is worth noting that fan anchors were capable of postponing plastic hinge formation by reducing the rate of increase in the plastic strain.

3.3.3 Strain Distribution

Strain distribution over the height of the FRP plate is plotted in Figs. 30 and 31 and compared at different loading stages. In all models, the first two loading stages (points 1 and 2) stand for the onset of debonding and the peak load of the unanchored model (S30-AM), respectively. To further investigate and compare the post-buckling response of the models, point 3 at 3.5 mm displacement was considered. Points 4, 5 and 6 correspond to FRP rupture, peak load

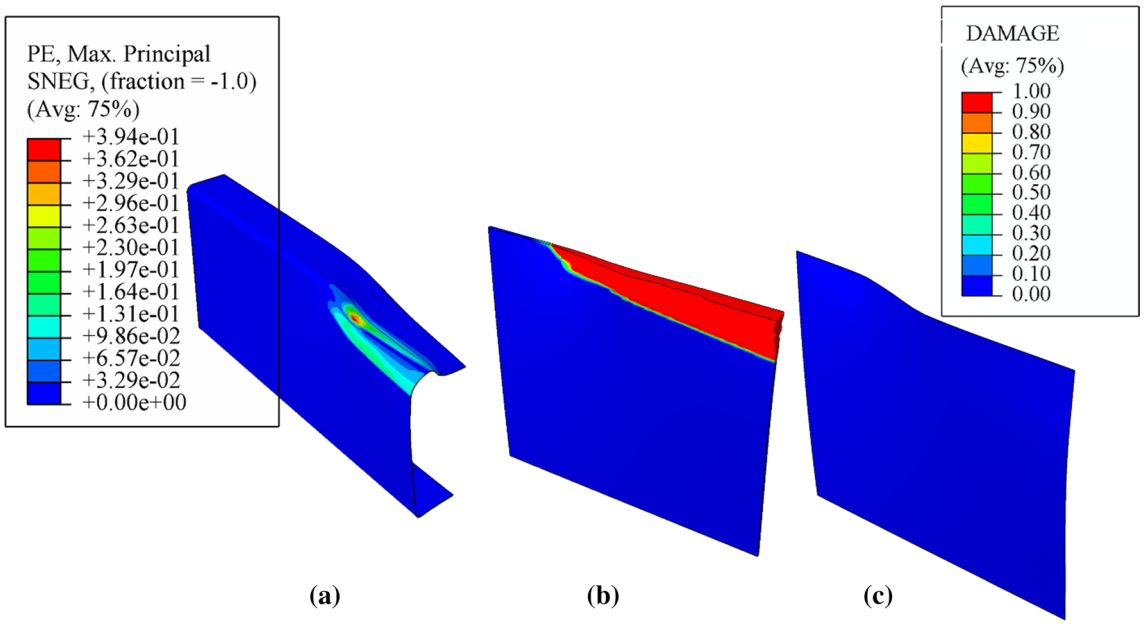

Fig. 28 S30-AM at failure: **a** plastic strain in the steel box, **b** damage status in the adhesive, and **c** damage status in the FRP plate

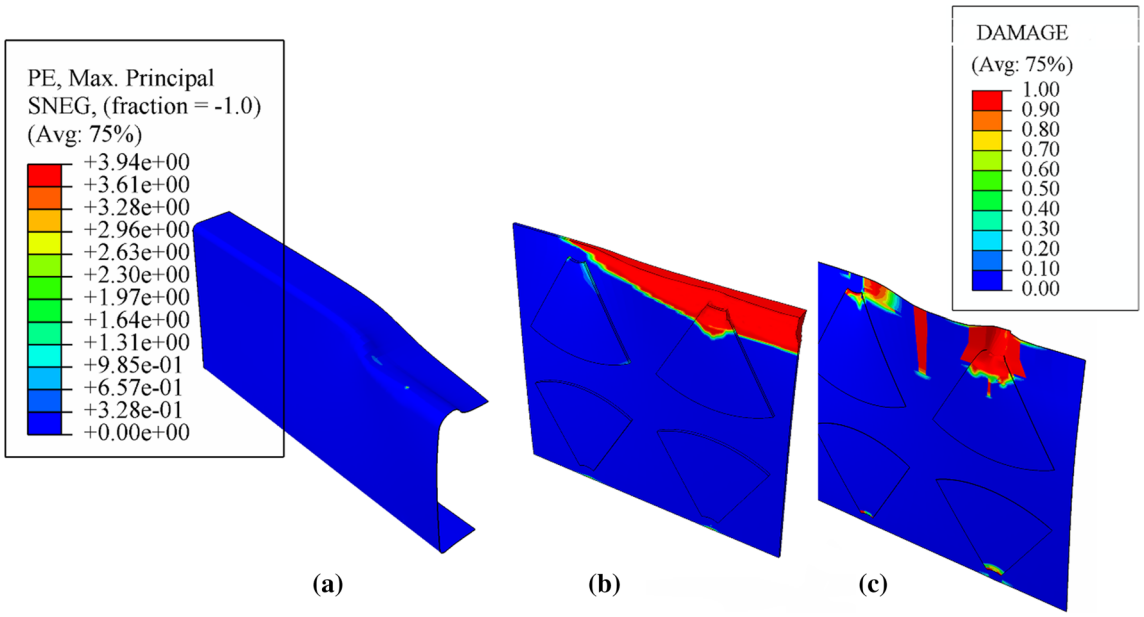

Fig. 29 S30-AM-4Anc at failure: **a** plastic strain in the steel box, **b** damage status in the adhesives and **c** damage status in the FRP plate and fan anchors

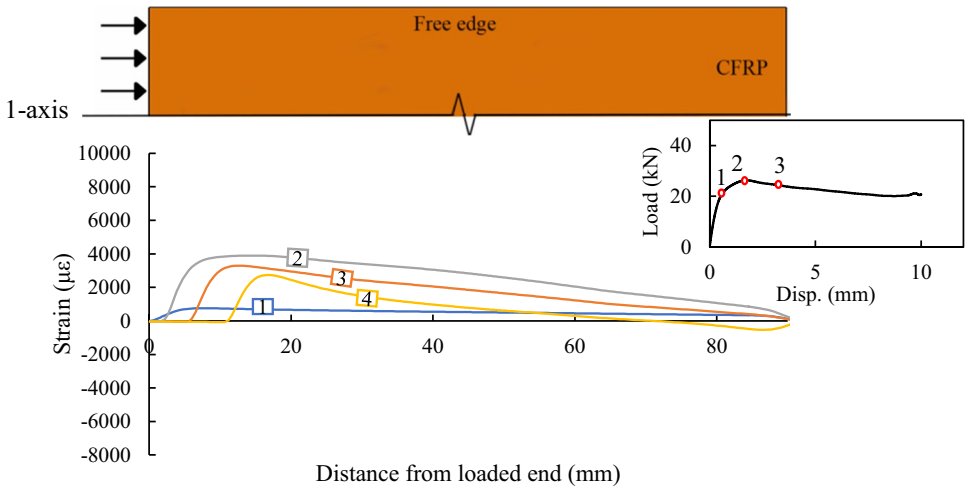

Fig. 30 Strain distribution in S30-AM model at different loading stages up to debonding

(anchor failure), and 20% strength loss in S30-AM-4Anc model, respectively. In these figures, the horizontal axis is along the 1-axis in Fig. 27, originating from the top edge of the FRP plate. Comparing Figs. 30 and 31 shows a significant alteration in the strain profile owing to the presence of fan anchors. In these graphs, zero strain corresponds to FRP debonding and discontinuity in strain represents FRP failure. By comparing the strain distribution of the two models at point 3, one can see that while more than 5 mm of FRP was debonded in the S30-AM, strain along the length of the FRP plate in the anchored model is non-zero, demonstrating the effect of anchorage system at precluding debonding.

In addition, at loading stages corresponding to points 4, 5, and 6 in the S30-AM-4Anc model, the strain distribution is interrupted by the rupture of FRP in the vicinity of the loaded end, which implies a full utilisation of the FRP strain capacity. The comparison of FRP strain in anchored and unanchored models is detailed in Table 8. As can be seen, FRP efficiency was significantly increased by the use of fan anchors.

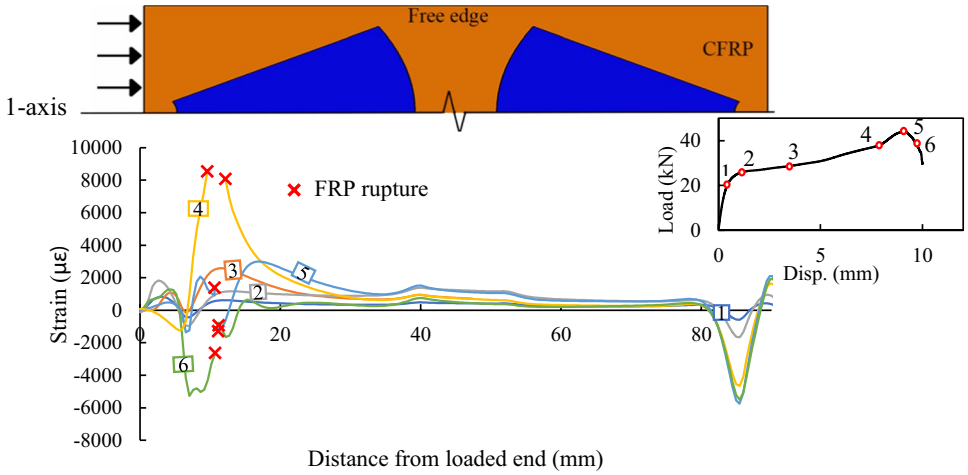

Fig. 31 Strain distribution in S30-AM-4Anc model at different loading stages up to debonding

4 Conclusion

The study presented in this paper proposed and evaluated the application of fan anchors in FRP-strengthened steel structures. Three experimental studies with different loading conditions were chosen for numerical investigation. After the validation of numerical models, fan anchors were added to the models and their efficiency in mitigating premature FRP debonding was assessed. In each numerical model, the effect of fan anchors and their quantity on the strength, failure mode and FRP plate's strain distribution were explored. Based on this numerical investigation, the following conclusions can be drawn:

- Employing fan anchors can considerably improve the FRP's overall performance in shear strengthening, flexural strengthening and buckling strengthening. In all anchored models, FRP debonding was postponed and a higher strengthening capacity was achieved.
- The effect of the number of fan anchors was investigated in shear strengthening and flexural strengthening examples. Increasing fan anchors from one row to two rows improved the performance of the anchorage system. However, due to an inadequate FRP anchorage length, increasing fan anchors from two to three pairs in flexurally strengthened beams did not yield a better FRP-to-steel bond performance.
- Compared to the other models, the increase in strength and strain capacities attained in anchored strengthened beams were lower. Nevertheless, fan anchors notably improved the ductility by preventing a significant decrease in the beam's load bearing during large deflections.
- Fan anchors were also capable of enhancing the strain efficiency of the FRP plate in all models. In the buckling strengthening, employing fan anchors resulted in fully exploiting the strengthening capacity of the FRP plate.
- In all anchored models, the strength reduction was due to the failure of anchors. Following the failure of fan anchors, the load dropped suddenly, and the load–displacement curve overlapped that of the unanchored models.

Funding No funding was received to assist with the preparation of this manuscript.

References

Alam, M. I., Fawzia, S., Zhao, X.-L., & Remennikov, A. M. (2017). Experimental study on FRP-strengthened steel tubular members under lateral impact. *Journal of Composites for Construction, 21*(5), 04017022. https://doi.org/10.1061/(ASCE)CC.1943-5614.0000801

American Concrete Institute (ACI). (2017). *Guide for the design and construction of externally bonded FRP systems for strengthening concrete structures* (ACI 440).

Benzeggagh, M. L., & Kenane, M. (1996). Measurement of mixed-mode delamination fracture toughness of unidirectional glass/epoxy composites with mixed-mode bending apparatus. *Composites Science and Technology, 56*(4), 439–449. https://doi.org/10.1016/0266-3538(96)00005-X

Buyukozturk, O., Gunes, O., & Karaca, E. (2004). Progress on understanding debonding problems in reinforced concrete and steel

members strengthened using FRP composites. *Construction and Building Materials, 18*(1), 9–19. https://doi.org/10.1016/S0950-0618(03)00094-1

da Silva, F. M. L., & Adams, D. R. (2007). Techniques to reduce the peel stresses in adhesive joints with composites. *International Journal of Adhesion and Adhesives, 27*(3), 227–235. https://doi.org/10.1016/j.ijadhadh.2006.04.001

del Rey Castillo, E., Dizhur, D., Griffith, M., & Ingham, J. (2019). Strengthening RC structures using FRP spike anchors in combination with EBR systems. *Composite Structures, 209*, 668–685. https://doi.org/10.1016/J.COMPSTRUCT.2018.10.093

Deng, J., & Lee, M. M. K. (2007). Behaviour under static loading of metallic beams reinforced with a bonded CFRP plate. *Composite Structures, 78*(2), 232–242. https://doi.org/10.1016/j.compstruct.2005.09.004

Deng, J., Lee, M. M. K., & Moy, S. S. J. (2004). Stress analysis of steel beams reinforced with a bonded CFRP plate. *Composite Structures, 65*(2), 205–215. https://doi.org/10.1016/J.COMPSTRUCT.2003.10.017

Faggiani, A., & Falzon, B. G. (2010). Predicting low-velocity impact damage on a stiffened composite panel. *Composites Part A: Applied Science and Manufacturing, 41*(6), 737–749. https://doi.org/10.1016/j.compositesa.2010.02.005

Fernando, D. (2010). *Bond behaviour and debonding failures in CFRP-strengthened steel members*. Hong Kong: The Hongkong Polythecnic University.

Fernando, D., Schumacher, A., Motavalli, M., Teng, J. G., Yu, T., & Ghafoori, E. (2010). Fatigue strengthening of cracked steel beams with CFRP plates. *ASME International Mechanical Engineering Congress and Exposition, 44465*, 271–276.

Hall, J. D., Schuman, P. M., & Hamilton, H. R., III. (2002). Ductile anchorage for connecting FRP strengthening of under-reinforced masonry buildings. *Journal of Composites for Construction, 6*(1), 3–10. https://doi.org/10.1061/(ASCE)1090-0268(2002)6:1(3)

Hashin, Z. (1980). Failure criteria for unidirectional fiber composites. *Journal of Applied Mechanics, 47*(2), 329–334. https://doi.org/10.1115/1.3153664

Kalfat, R., Al-Mahaidi, R., & Smith, S. T. (2013). Anchorage devices used to improve the performance of reinforced concrete beams retrofitted with FRP composites: State-of-the-art review. *Journal of Composites for Construction, 17*(1), 14–33. https://doi.org/10.1061/(ASCE)CC.1943-5614.0000276

Katrizadeh, E., & Narmashiri, K. (2019). Experimental study on failure modes of MF-CFRP strengthened steel beams. *Journal of Constructional Steel Research, 158*, 120–129. https://doi.org/10.1016/j.jcsr.2019.03.027

Li, J., Wang, Y., Deng, J., & Jia, Y. (2018). Experimental study on the flexural behaviour of notched steel beams strengthened by prestressed CFRP plate with an end plate anchorage system. *Engineering Structures, 171*, 29–39. https://doi.org/10.1016/j.engstruct.2018.05.042

Liu, Z. Q., Luo, B., Wang, Q., & Feng, B. (2021). Experimental and numerical investigation of the anti-debonding performance for novel CFRP-steel tube composite member under tension. *Journal of Building Engineering, 35*, 102004. https://doi.org/10.1016/J.JOBE.2020.102004

Naser, M. Z., Hawileh, R. A., & Abdalla, J. A. (2019). Fiber-reinforced polymer composites in strengthening reinforced concrete structures: A critical review. *Engineering Structures, 198*, 109542. https://doi.org/10.1016/j.engstruct.2019.109542

Park, R. (1989). Evaluation of ductility of structures and structural assemblages from laboratory testing. *Bulletin of the New Zealand Society for Earthquake Engineering, 22*(3), 155–166. https://doi.org/10.5459/bnzsee.22.3.155-166

Schnerch, D., Dawood, M., Rizkalla, S., & Sumner, E. (2007). Proposed design guidelines for strengthening of steel bridges with FRP materials. *Construction and Building Materials, 21*(5), 1001–1010. https://doi.org/10.1016/J.CONBUILDMAT.2006.03.003

Sen, R., Liby, L., & Mullins, G. (2001). Strengthening steel bridge sections using CFRP laminates. *Composites Part B: Engineering, 32*(4), 309–322. https://doi.org/10.1016/S1359-8368(01)00006-3

Shaat, A., & Fam, A. (2006). Axial loading tests on short and long hollow structural steel columns retrofitted using carbon fibre reinforced polymers. *Canadian Journal of Civil Engineering, 33*(4), 458–470. https://doi.org/10.1139/L05-042

Shadan, F., Khaloo, A., & Shadan, P. (2015). Numerical study on flexural strengthening of squat RC shear wall using FRP laminates. *Scientia Iranica*, *22*(1).

Shadan, P., & Kabir, M. Z. (2018). Enhancing local buckling behavior of SHS braces using GFRP and CFRP wrap. *Journal of Composites for Construction*. https://doi.org/10.1061/(ASCE)CC.1943-5614.0000850

Shadan, P., & Kabir, M. Z. (2018b). Experimental and numerical investigation of FRP-confined SHS brace members under cyclic loading. *Thin-Walled Structures*. https://doi.org/10.1016/j.tws.2018.04.021

Shadan, P., & Kabir, M. Z. (2018). Effect of FRP strengthening on the SHS brace collapse mechanism. *Scientia Iranica*. https://doi.org/10.24200/sci.2018.20690

Sivaganesh, S., & Mahendrakumar, M. (2019). Strengthening of laterally restrained steel beams subjected to flexural loading using low-modulus CFRP. *Journal of Performance of Constructed Facilities, 33*(3), 4019032. https://doi.org/10.1061/(ASCE)CF.1943-5509.0001293

Smith, S. T., & Teng, J. G. (2001). Interfacial stresses in plated beams. *Engineering Structures, 23*(7), 857–871. https://doi.org/10.1016/S0141-0296(00)00090-0

Sweedan, A. M. I., El-Sawy, K. M., & Alhadid, M. M. A. (2013). Interfacial behavior of mechanically anchored FRP laminates for strengthening steel beams. *Journal of Constructional Steel Research, 80*, 332–345. https://doi.org/10.1016/j.jcsr.2012.09.022

Sweedan, A. M. I., Alhadid, M. M. A., & El-Sawy, K. M. (2016). Experimental study of the flexural response of steel beams strengthened with anchored hybrid composites. *Thin-Walled Structures, 99*, 1–11. https://doi.org/10.1016/j.tws.2015.10.026

Teng, J. G., Yu, T., & Fernando, D. (2012). Strengthening of steel structures with fiber-reinforced polymer composites. *Journal of Constructional Steel Research, 78*, 131–143. https://doi.org/10.1016/j.jcsr.2012.06.011

Tsouvalis, N. G., Mirisiotis, L. S., & Dimou, D. N. (2009). Experimental and numerical study of the fatigue behaviour of composite patch reinforced cracked steel plates. *International Journal of Fatigue, 31*(10), 1613–1627. https://doi.org/10.1016/J.IJFATIGUE.2009.04.006

Wang, Y., & Zhou, C. (2017). Bond Characteristics of CFRP/Steel Interface End-anchored with G-shaped Clamps. *Polymers and Polymer Composites, 25*(9), 661–668. https://doi.org/10.1177/096739111702500903

Wang, B., Bai, Y., Hu, X., & Lu, P. (2016). Enhanced epoxy adhesion between steel plates by surface treatment and CNT/short-fibre reinforcement. *Composites Science and Technology, 127*, 149–157. https://doi.org/10.1016/j.compscitech.2016.03.008

Wang, Q., Zhu, H., Zhang, B., Tong, Y., Teng, F., & Su, W. (2020). Anchorage systems for reinforced concrete structures strengthened with fiber-reinforced polymer composites: State-of-the-art review. *Journal of Reinforced Plastics and Composites, 39*(9–10), 327–344. https://doi.org/10.1177/0731684420905010

Yang, Y., Zhao, J., Zhang, S., Chastre, C., & Biscaia, H. (2021). Effect of mechanical anchorage on the bond performance of double overlapped CFRP-to-steel joints. *Composite Structures, 267*, 113902. https://doi.org/10.1016/j.compstruct.2021.113902

Yazdani, N., Aljaafreh, T., & Beneberu, E. (2020). Concrete beam flexural strengthening with anchored pre-saturated CFRP laminates. *Composite Structures, 235*, 111733. https://doi.org/10.1016/j.compstruct.2019.111733

Yu, Q.-Q., & Wu, Y.-F. (2018). Fatigue behaviour of cracked steel beams retrofitted with carbon fibre–reinforced polymer laminates. *Advances in Structural Engineering, 21*(8), 1148–1161. https://doi.org/10.1177/1369433217729518

Yu, T., Fernando, D., Teng, J. G., & Zhao, X. L. (2012). Experimental study on CFRP-to-steel bonded interfaces. *Composites Part B: Engineering, 43*(5), 2279–2289. https://doi.org/10.1016/j.compositesb.2012.01.024

Zhang, H. W., & Smith, S. T. (2012). FRP-to-concrete joint assemblages anchored with multiple FRP anchors. *Composite Structures, 94*(2), 403–414. https://doi.org/10.1016/j.compstruct.2011.07.025

Zhang, H. W., Smith, S. T., & Kim, S. J. (2012). Optimisation of carbon and glass FRP anchor design. *Construction and Building Materials, 32*, 1–12. https://doi.org/10.1016/j.conbuildmat.2010.11.100

Zhao, X. L., & Zhang, L. (2007). State-of-the-art review on FRP strengthened steel structures. *Engineering Structures, 29*(8), 1808–1823. https://doi.org/10.1016/j.engstruct.2006.10.006

Zheng, Z., Du, Y., Chen, Z., Li, S., & Niu, J. (2021). Experimental and theoretical studies of FRP-Steel composite plate under static tensile loading. *Construction and Building Materials, 271*, 121501. https://doi.org/10.1016/j.conbuildmat.2020.121501